Accepted to Geotechnique 28/05/2021

Probabilistic failure envelopes of strip foundations on soils with non-stationary characteristics of undrained shear strength

Zhichao Shen[1,2], Qiujing Pan[3,*], Siau Chen Chian[2], Susan Gourvenec[4], Yinghui Tian[5]

1. State Key Laboratory of Hydraulic Engineering Simulation and Safety, Tianjin University, China
2. Department of Civil and Environmental Engineering, National University of Singapore, Singapore
3. School of Civil Engineering, Central South University, China
4. School of Engineering, University of Southampton, UK
5. Department of Infrastructure Engineering, University of Melbourne, Australia

Zhichao SHEN, Research Fellow

Email: ceesz@nus.edu.sg

Qiujing PAN (*Corresponding author), Professor

School of Civil Engineering

Central South University

No.22, Shaoshan South Road, Changsha, Hunan 410075

China

Email: qiujing.pan@csu.edu.cn

Siau Chen CHIAN, Associate professor

Email: sc.chian@nus.edu.sg

Susan GOURVENEC, Professor

Email: Susan.Gourvenec@southampton.ac.uk

Yinghui TIAN, Associate professor

Email: yinghui.tian@unimelb.edu.au

No. of words: 5348 (excluding abstract and references)

No. of tables: 3

No. of figures: 16

Probabilistic failure envelopes of strip foundations on soils with non-stationary characteristics of undrained shear strength

Zhichao Shen[1,2], Qiujing Pan[3,*], Siau Chen Chian[2], Susan Gourvenec[4], Yinghui Tian[5]

Abstract

This paper investigates the probabilistic failure envelopes of strip foundations on spatially variable soils with a profile of undrained shear strength s_u increasing with depth using the lower bound random finite element limit analysis. The spatially variable s_u is characterised by a non-stationary random field with linearly increasing mean and constant coefficient of variation (COV) with depth. The deterministic uniaxial capacities and failure envelopes are firstly derived to validate numerical models and provide a reference for the subsequent probabilistic analysis. Results indicate that the random field parameters COV_{su} (COV of s_u) and Δ (dimensionless autocorrelation distance) have a considerable effect on the probabilistic normalised uniaxial capacities which alters the size of probabilistic failure envelopes. However, an insignificant effect on the shape of probabilistic failure envelopes is observed in the V-H, V-M and H-M loading spaces, such that the failure envelopes for different soil variabilities can be simply scaled. In comparison to COV_{su} and Δ, the soil heterogeneity index $\kappa = \mu_k B/\mu_{su0}$ has the lowest effect on probabilistic normalised uniaxial capacity factors but the highest effect on the shape of probabilistic failure envelopes. The autocorrelation function models have minimal influence on both size and shape of probabilistic failure envelopes. A series of expressions are proposed to describe the shape of deterministic and probabilistic failure envelopes for strip foundations under combined vertical, horizontal and moment (V-H-M) loading.

Keywords: Probabilistic analysis; Footings/foundations; Failure envelopes; Soil spatial variability; Sparse polynomial chaos expansion/global sensitivity analysis

List of notations:

$\boldsymbol{A}$	index set of PCE
B	width of strip foundation
COV	coefficient of variation of a variable
E_{u}	undrained Young's modulus
F_{u}	failure load
$F_{\mathrm{u,p}}$	quantile of failure load
$\boldsymbol{G}$	random field of a variable
H	horizontal load
$H_{\mathrm{u,det}}$	deterministic horizontal ultimate capacity
$H_{\mathrm{u,ran}}$	random horizontal ultimate capacity
$H_{\mathrm{u,p}}$	quantile of horizontal ultimate capacity
h	deterministic normalised horizontal load
h_{p}	random normalised horizontal load
h_{u}	normalised horizontal capacity
$h_{\mathrm{u,p}}$	quantile of normalised horizontal capacity
k	gradient of undrained shear strength profile with depth
$k_{\boldsymbol{\alpha}}$	coefficient of PCE
$\boldsymbol{k'}$	estimated column vector of coefficients of PCE
L	number of random variables used for generation of random field
L'	number of selected significant random variables according to corresponding Sobol indices
l	number of data points
M	moment
$M_{\mathrm{u,det}}$	deterministic moment ultimate capacity
$M_{\mathrm{u,ran}}$	random moment ultimate capacity
$M_{\mathrm{u,p}}$	quantile of moment ultimate capacity
m	deterministic normalised moment load
m_{p}	random normalised moment load
m_{u}	normalised moment capacity
$m_{\mathrm{u,p}}$	quantile of normalised moment capacity
N	number of realizations of random field
n	PCE order
n_{max}	maximum PCE order
P	total number of elements in the index set A
p	probability
R^2	coefficient of determination
R^2_{tgt}	target accuracy of coefficient of determination
$S(\zeta_i)$	first-order Sobol index for a single variable ζ_i
s_{u}	undrained shear strength
s_{u0}	undrained shear strength at the mudline
t	trend function
V	vertical load
$V_{\mathrm{u,ran}}$	random vertical ultimate capacity
$V_{\mathrm{u,det}}$	deterministic vertical ultimate capacity
$V_{\mathrm{u,p}}$	quantile of vertical ultimate capacity
v	deterministic normalised vertical load
v_{p}	random normalised vertical load

v_u normalised vertical capacity
$v_{u,p}$ quantile of normalised vertical capacity
Y system response
$\boldsymbol{Y'}$ N realizations of system response based on finite element analysis
z depth below ground surface
$\boldsymbol{\alpha}$ L dimensional index
δ autocorrelation distance
δ_h horizontal autocorrelation distance
δ_v vertical autocorrelation distance
Δ dimensionless autocorrelation distance
Δ_h dimensionless horizontal autocorrelation distance
Δ_v dimensionless vertical autocorrelation distance
ε fluctuating residuals
ε_{cut} cut-off value of PCE
η soil property
κ soil heterogeneity index
μ mean of a variable
ν Poisson ratio
θ scale of fluctuation
ρ autocorrelation function
σ standard deviation of a variable
$\Psi_{\boldsymbol{\alpha}}(\boldsymbol{\zeta})$ multivariate polynomials of PCE
$\boldsymbol{\zeta}$ independent standard random vector

1. Introduction

Offshore shallow foundations are typically subject to combined vertical *V*, horizontal *H* and moment *M* loading and in many regions rest on normally consolidated and lightly over-consolidated marine clay deposits with increasing undrained shear strength s_u with depth (Fig. 1). There has been increasing popularity of defining the load-carrying capacity of offshore shallow foundations as a failure envelope bounded in terms of combined V-H-M loading. Undrained failure envelopes of shallow foundations for various geometries, such as strip (Bransby & Randolph, 1998; Gourvenec & Randolph, 2003; Gourvenec, 2008; Gourvenec & Barnett, 2011; Vulpe *et al*., 2016, Xiao *et al*., 2016, Shen *et al.*, 2016), circular (Taiebat & Carter, 2000; Gourvenec, 2007; Vulpe *et al*. 2016, 2017, Shen *et al.*, 2017a) and rectangular (Feng *et al.*, 2014; Feng *et al.*, 2017; Shen *et al.*, 2017b), have been investigated rigorously under different ground conditions and foundation geometry (e.g., soil strength non-homogeneity, strain softening, embedment depth and soil-foundation interface condition).

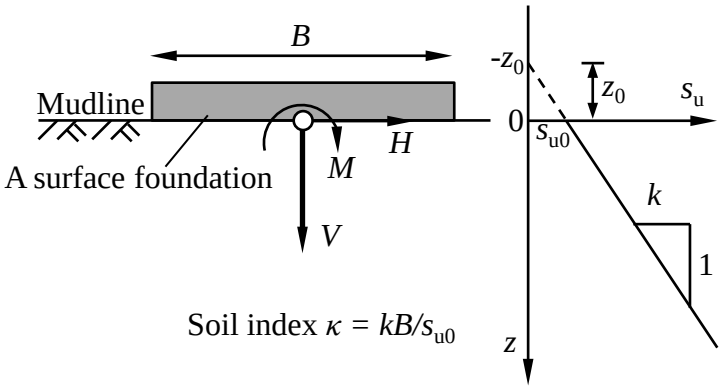

Fig. 1. Convention for foundation loads and soil strength profiles, positive load directions shown

However, these failure envelopes have been derived based on a deterministic approach without considering spatial variability of the soil strength. In practice, in situ soil properties vary vertically and horizontally due to natural geologic processes, and inherent soil variability can be concisely modelled as a ‘random field’ described by an autocorrelation function model ρ

and parameters including the mean μ, standard deviation σ (or coefficient of variation *COV*) and scale of fluctuation θ (Phoon & Kulhawy, 1999; Uzielli *et al*. 2007). A random field is a random (or stochastic) process consisting of an indexed (i.e., could be one or more reference dimensions) set of random variables (Vanmarcke 1983).

Statistical characterisation of soil spatial variability depends heavily on the hypothesis of data stationarity. A soil profile is considered to be stationary if: 1) the mean μ and standard deviation σ do not vary with depth and 2) the autocovariance at two different depths z_i and z_j is only a function of their distance $|z_i - z_j|$, rather than their absolute position z_i and z_j (Phoon & Kulhawy, 1999; Phoon *et al.*, 2003; Li *et al.*, 2015). Note that for a soil profile, stationarity or statistical homogeneity can be identified by modified Bartlett test statistics (Phoon et al., 2003). For a non-stationary data set, data transformation should be carried out to define a stationary data set. Trend removal is the most common way to achieve a stationary data set, which can be carried out by least square regression analysis (Phoon & Kulhawy, 1999; Phoon *et al.*, 2003; Uzielli *et al.*, 2005; Stuedlein *et al.*, 2012). For illustration, Fig. 2 shows a non-stationary soil profile in the vertical direction. The soil property $\eta(z)$ may be decomposed into a deterministic trend function $t(z)$ and a randomly fluctuating residuals $\varepsilon(z)$ as

$$\eta(z) = t(z) + \varepsilon(z) \tag{1}$$

where z is the depth. The linear trend t(z) is a function of the depth z and thus a non-stationary component. The fluctuating residuals $\varepsilon(z)$ representing the inherent soil variability can be modelled by a stationary random field. For the stationary random field $\varepsilon(z)$, the mean μ_ε and standard deviation σ_ε can be directly estimated based on the fluctuation

$$\mu_\varepsilon = \frac{1}{l}\sum_{i=1}^{l} \varepsilon\left(z_i\right) \tag{2a}$$

$$\sigma_{\varepsilon} = \sqrt{\frac{1}{l}\sum_{i=1}^{l}\left[\varepsilon\left(z_i\right) - \mu_{\varepsilon}\right]^2} \tag{2b}$$

where l is the number of data points, and $\varepsilon(z_i)$ is the fluctuation at depth z_i. μ_{ε} is a constant value of zero due to equal fluctuations on the two sides of the trend line (Phoon & Kulhawy, 1999). Eq. (2b) is a biased estimator as it is not divided by $l - 1$. Fenton (1999) explained the reasons for the adoption of a biased estimator. The scale of fluctuation θ as another random field parameter describes the distance over which the soil properties are similar or correlated, which can be estimated by several methods, including method of moments (Uzielli *et al.*, 2005; Stuedlein *et al.*, 2012; Cami *et al.*, 2020), maximum-likelihood estimation (Degroot & Baecher, 1993; Liu & Leung, 2018; Xiao *et al.*, 2018) and Bayesian analysis (Wang *et al.*, 2010; Ching *et al.*, 2016; Tian *et al.*, 2016). Based on statistics of $\varepsilon(z)$, the mean μ_{η} and standard deviation σ_{η} of the non-stationary random field $\eta(z)$ can be obtained

$$\mu_{\eta} = t(z) \tag{3a}$$

$$\sigma_{\eta} = \sigma_{\varepsilon} \tag{3b}$$

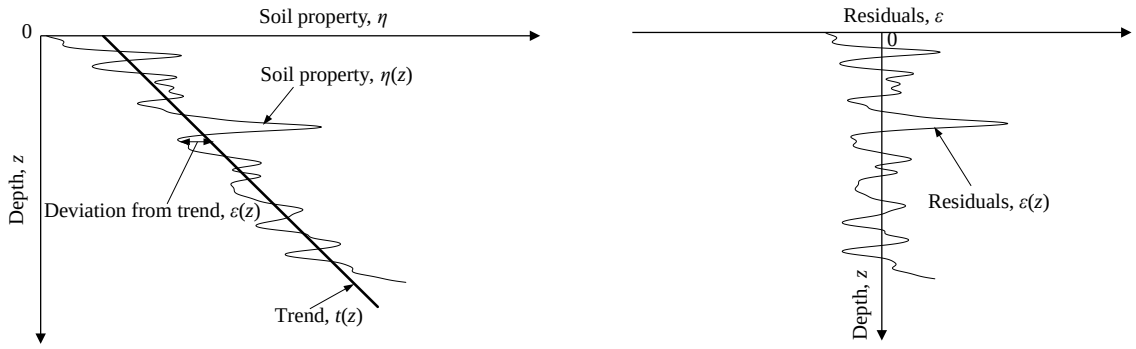

(a) profile of soil property and the trend (b) detrended soil property (residuals)

Fig. 2. Decomposition of nonstationary soil property

Given the prevalence of soil spatial variability, it is of keen interest to investigate the effect of spatially variable soil properties on the load-carrying capacities of shallow foundations.

To date, most studies of shallow foundations on spatially variable soils focus on the probabilistic pure vertical capacity (Griffiths & Fenton, 2001; Griffiths *et al.*, 2002; Popescu *et al.*, 2005; Kasama & Whittle, 2011; Li *et al.*, 2015; Jha Sanjay, 2016; Shen *et al.*, 2020). These studies have shown that the presence of soil spatial variability results in the mean capacity in the probabilistic case lower than the deterministic case. Probabilistic failure envelopes of surface strip foundations (Cassidy *et al.*, 2013; Hentati *et al.*, 2018; Shi *et al.*, 2019) and skirted foundations (Selmi *et al.*, 2019) have been investigated for soils with constant mean μ_{su} and standard deviation σ_{su} of undrained shear strength (see Fig. 3a), which can be characterised by a 'stationary random field'. However, for typically normally consolidated or lightly over-consolidated seabed clays, the mean shear strength μ_{su} increases with depth, exhibiting a non-stationary characteristic. A 'non-stationary random field' is capable of characterising the linearly increasing μ_{su} and σ_{su} with depth as illustrated in Fig. 3b (Yi *et al.*, 2020). Charlton & Rouainia (2017) explored probabilistic failure envelopes of skirted foundations on soils represented by a non-stationary random field, but neglected variation of undrained shear strength at the mudline s_{u0} (i.e., $\sigma_{su} = 0$ at $z = 0$, see Fig. 3c) such that horizontal capacities of surface foundations are nearly constant irrespective of soil spatial variability. Shen *et al.* (2020) propose a simple but effective method to produce a non-stationary random field that can consider the variation of shear strength at the mudline, as described in Fig. 3b, where the mean μ_{su} and standard deviation σ_{su} of undrained shear strength can be efficiently controlled in the proposed non-stationary random field.

This paper investigates probabilistic failure envelopes of strip foundations on soils characterised by both stationary and non-stationary random fields. The effect of soil parameters, including the soil heterogeneity index κ, the coefficient of variation COV of shear strength s_u

and the dimensionless autocorrelation distance Δ, on the size and shape of probabilistic failure envelopes are discussed.

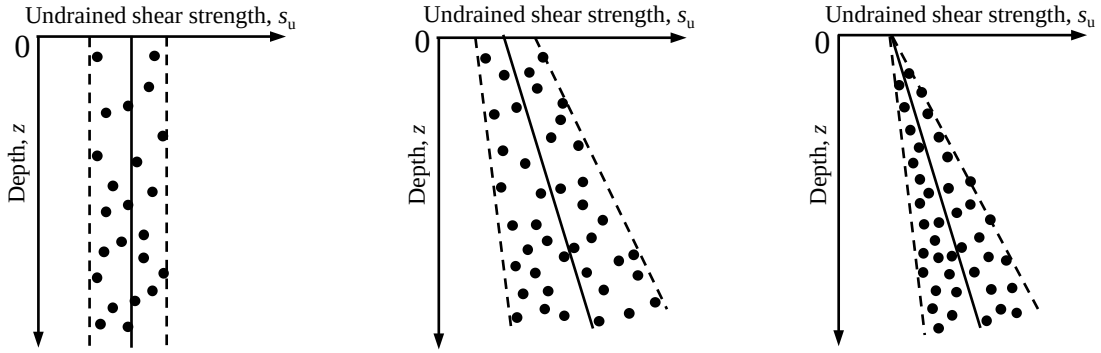

(a) constant μ_{su} and σ_{su} with depth z

(b) μ_{su} and σ_{su} increasing with depth z ($\sigma_{su} \neq 0$ at z =0)

(c) μ_{su} and σ_{su} increasing with depth z (σ_{su} = 0 at z =0)

Fig. 3. Characterization of different types of spatial variability of undrained shear strength

Numerical analyses were carried out with lower bound (LB) random finite element limit analysis (RFELA), in OPTUM G2 (Krabbenhoft, 2019a). In order to maintain an acceptable computation time, a surrogate model was established using the 'sparse polynomial chaos expansion/global sensitivity analysis' (SPCE/GSA) method (Al-Bittar & Soubra, 2014; Pan & Dias, 2017; Guo *et al.*, 2019). A significant amount of time has been saved within a Monte Carlo (MC) framework of SPCE/GSA analyses rather than conducting all cases by using RFELA simulations (which are relatively time-consuming). Although the SPCE/GSA technique was adopted, more than 531,000 RFELA simulations were carried out for the probabilistic analysis in this study. A single RFELA simulation took approximately 10 seconds on the authors' computer (3.2 GHz CPU and 16 GB memory).

2. The random field of undrained shear strength

Undrained shear strength s_u that linearly increases with depth can be expressed as

$$s_u = s_{u0} + kz = k(z + z_0) \quad (4)$$

where s_{u0} is the undrained shear strength at the mudline, k is the gradient of shear strength profile with depth, and z_0 is a constant, $z_0 = s_{u0}/k$. It is noteworthy that for normally consolidated marine clay s_{u0} is often a near zero value, resulting in a minor value of z_0.

Based on Eq. (4), a non-stationary random field of the undrained shear strength $\boldsymbol{G}_{\mathbf{su}}$ can be generated as the product of the stationary random field $\boldsymbol{G}_{\mathbf{k}}$ of the gradient k and the equivalent depth $(z + z_0)$ (see Shen *et al.*, 2020 for details about the method), expressed as

$$\boldsymbol{G}_{\mathbf{su}} = \boldsymbol{G}_{\mathbf{k}}(z + z_0) \tag{5}$$

The statistical parameters of s_u, including mean μ_{su}, standard deviation σ_{su} and coefficient of variation COV_{su}, can be calculated using the following equations:

$$\mu_{su} = \mu_k(z + z_0) \tag{6a}$$

$$\sigma_{su} = \sigma_k(z + z_0) \tag{6b}$$

$$COV_{su} = \sigma_{su}/\mu_{su} = \sigma_k/\mu_k = COV_k \tag{6c}$$

where μ_k, σ_k and COV_k are the statistical parameters for the gradient k that follow definitions for s_u.

The stationary random fields $\boldsymbol{G}_{\mathbf{k}}$ and $\boldsymbol{G}_{\mathbf{su}}$ are assumed to be log-normally distributed (Griffiths & Fenton, 2001) in this study, which can be produced by the covariance matrix decomposition method (CMDM) (Davis, 1987; Kasama & Whittle, 2011; Zhang *et al*., 2016). The covariance matrix is constructed with a typical squared exponential autocorrelation function ρ.

$$\rho = \exp\left[-\left(\frac{x_i - x_j}{\delta_h}\right)^2 - \left(\frac{z_i - z_j}{\delta_v}\right)^2\right] \tag{7}$$

where (x_i, z_i) and (x_j, z_j) are two points of the random field. δ_h and δ_v denote the horizontal and vertical autocorrelation distances. Note that for this type of autocorrelation function, the relationship between the scale of fluctuation θ and autocorrelation distance δ can be expressed

as $\theta = \sqrt{\pi}\delta$. The procedure to generate a stationary random field using CMDM was introduced in detail by Shen *et al*. (2020).

According to Phoon & Kulhawy (1999), Duncan (2000) and Griffiths & Fenton (2001), the recommended range of *COV* of undrained shear strength COV_{su} was set between 0.1 – 0.5. Keaveny *et al.* (1989) and Phoon and Kulhawy (1999) reported a similar range of vertical scale of fluctuation of s_u, in the region of 0.48 – 7.14 m and 0.8 – 6.2 m, respectively. The horizontal scale of fluctuation can be tenfold larger than that in the vertical direction (Phoon & Kulhawy, 1999; Li *et al.*, 2016).

In deterministic cases, the degree of soil heterogeneity for profiles of linearly increasing s_u with depth is typically represented by the dimensionless soil index $\kappa = kB/s_{u0}$. For consistency, $\kappa = \mu_k B/\mu_{su0}$ is adopted in probabilistic cases. A simple form of $\kappa = B/z_0$ can be obtained based on the relationship of $\mu_{su0} = \mu_k z_0$. Under this definition, $\kappa = 0$ infers a stationary random field of shear strength, and $\kappa > 0$ corresponds to the non-stationary cases.

In this paper, a strip foundation of width $B = 2$ m rests on the soil with a vertical autocorrelation distance of $\delta_v = 1$ m, resulting in the dimensionless vertical autocorrelation distance $\Delta_v = \delta_v/B = 0.5$. The ratio of horizontal and vertical autocorrelation distance $\Delta_h/\Delta_v = 5$ is maintained to represent the anisotropic property of the random field. The ranges of κ and COV_{su} adopted in the parametric analysis presented in this study are: $\kappa = 0, 2, 6, 10$, $COV_{su} = 0.1, 0.3, 0.5$. The effect of dimensionless autocorrelation distance Δ on probabilistic uniaxial capacities and failure envelopes is also investigated at $COV_{su} = 0.3$.

3. Numerical model

3.1. Geometry and mesh

All the numerical analyses were performed using the software OPTUM G2 (Krabbenhoft, 2019a). The undrained response of a strip foundation of width B = 2 m resting on the surface of a clay deposit was modelled. The soil domain boundaries extended a distance of 3B from the edge of foundation and 3B beneath the foundation, providing sufficient area for failure mechanisms to be mobilised. Elements of the type *Lower* were used to conduct the LB RFELA. The mesh with 3 adaptive refinement steps started with 1000 elements and ended with 2000 elements, which was tested and shown to be a good balance between computation effort and accuracy. The *Shear Dissipation* mode was adopted for the adaptivity control, which is generally the most efficient and reliable for such limit analysis (Krabbenhoft, 2019a). This means that a total of 3 calculations were carried out in one LB RFELA, and the mesh is adapted according to the previous distribution of the shear dissipation in the last calculation. Fig. 4 shows the adaptive mesh for the foundation on uniform soil under a vertical load. As particularly useful tools for the *Lower* type elements, Mesh Fan can be applied to a point to create 'fan' of elements around it to improve the accuracy of results, which can be seen from the boxed and amplified region in Fig. 4. Based on the comparison of a range of *Fan Angle* and *Max Mesh Size*, features of Mesh Fan (*Fan Angle* = 20°) and Mesh Size (*Max Mesh Size* = 0.01B) were applied to two points at the corner of the foundation (Krabbenhoft, 2019b). The accuracy of LB FELA is summarised in Table 2.

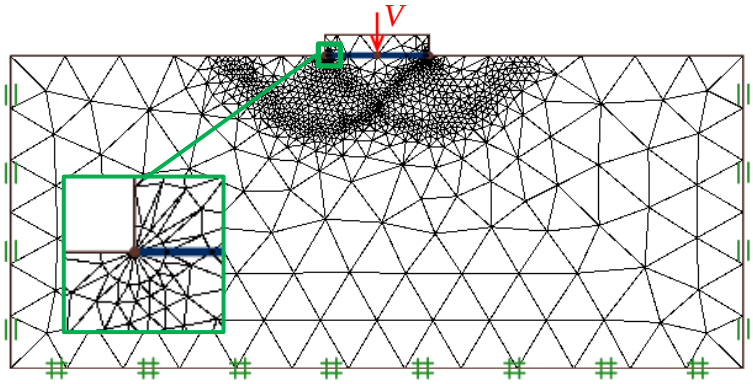

Fig. 4. Finite element mesh (example shown for vertically loaded foundation on uniform soil)

3.2. Material properties and interface conditions

A linear elastic perfectly plastic constitutive law obeying the Tresca failure criterion was used to represent undrained soil behaviour. The distribution of undrained shear strength s_u in the soil domain was simulated by the random field $\boldsymbol{G}_{\mathbf{su}}$. A constant modulus ratio of E_u/s_u =1000 was maintained (Gourvenec & Randolph, 2003; Cassidy *et al.*, 2013; Hentati *et al.*, 2018) and a Poisson's ratio of $\nu = 0.49$ was used to approximate a constant volume response of soil under undrained conditions. The effect of soil elastic parameters on ultimate capacities of shallow foundations is negligible (Bransby & Randolph, 1998; Cassidy *et al.*, 2013). The strip foundation was considered as a weightless rigid body with the reference point located at the midpoint of the foundation underside. The interface between soil and foundation base was assumed to be fully rough in shear with no separation permitted (i.e., fully bonded).

The soil domain was represented with a group of discrete grid points with 50 horizontally equidistant points in each row and 20 vertically equidistant points in each column. The random field of undrained shear strength $\boldsymbol{G}_{\mathbf{su}}$ was generated at these grid points using CMDM method. The generated random field $\boldsymbol{G}_{\mathbf{su}}$ was mapped into the FE model through coordinates of grid points and corresponding random field values using the *Map* option (Krabbenhoft, 2019c). Fig. 5 shows two examples to illustrate the distribution of s_u in stationary and non-stationary random

fields, respectively. Compared to the random distribution of s_u in the stationary random field, the soil strength s_u displays a trend of increasing with depth in the non-stationary random field.

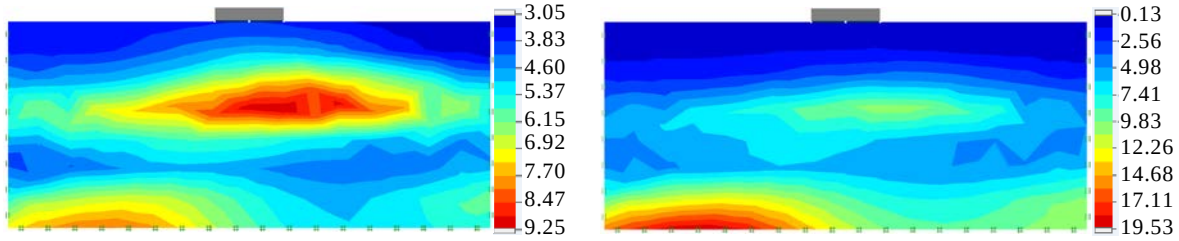

(a) COV_{su} = 0.3, κ = 0, μ_{su} = 5.0 kPa (stationary)

(b) COV_{su} = 0.5, κ = 10, μ_{su0} = 0.3 kPa, μ_k = 1.5 kPa/ m (non-stationary)

Fig. 5. Realisations of random fields of undrained shear strength s_u

3.3. Loading paths

Load-controlled probe tests were used to detect failure envelopes. Varying fixed ratios of VH, VM and HM loads were applied to the reference point of the shallow foundation to obtain corresponding load combinations at failure. *Multiplier* loads (Krabbenhoft, 2019b) with a uniform magnitude of unity and varying orientations with 10° increments in the normalised load space were adopted in the LB analysis so that fixed ratios of loads were maintained, as shown in Fig. 6.

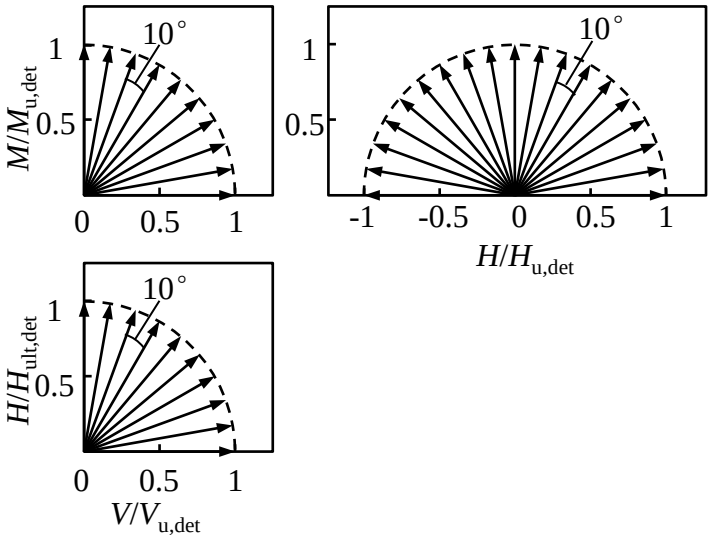

Fig. 6. Example of load-controlled probe tests to detect failure envelopes

3.4. Sign convention and notation

Fig. 1 shows the sign convention for loads adopted in this study. The notations for loads and ultimate capacities are summarised in Table 1. Both deterministic and random uniaxial ultimate capacities are derived under one single pure loading (e.g., $V = H = 0$ for $M_{u,det}$ and $M_{u,ran}$). A random uniaxial ultimate capacity (e.g., $V_{u,ran}$) is a random variable and its realisations are obtained through the MC simulation. The quantile of uniaxial ultimate capacity $V_{u,p}$ (or $H_{u,p}$ and $M_{u,p}$) corresponding to a given probability p refers to the value satisfying the probability $P(V_{u,ran} \leq V_{u,p}) = p$. For example, $V_{u,5\%}$ (the given probability p = 5%) is the 5% lower bound of the random vertical capacity. Corresponding to the random vertical ultimate capacity $V_{u,ran}$, the normalised vertical capacity v_u is also a random variable, and $v_{u,p}$, μ_{vu}, COV_{vu} are its quantile, mean and coefficient of variation, respectively. The same applies to horizontal and moment loadings.

Table 1 Summary of notations for loads and ultimate capacities

	Vertical	Horizontal	Moment
Load	V	H	M
Deterministic uniaxial ultimate capacity	$V_{u,det}$	$H_{u,det}$	$M_{u,det}$
Random uniaxial ultimate capacity	$V_{u,ran}$	$H_{u,ran}$	$M_{u,ran}$
Quantile of uniaxial ultimate capacity	$V_{u,p}$	$H_{u,p}$	$M_{u,p}$
Deterministic dimensionless load	V/Bs_{u0}	H/Bs_{u0}	M/B^2s_{u0}
Deterministic normalised load	$v = V/V_{u,det}$	$h = H/H_{u,det}$	$m = M/M_{u,det}$
Probabilistic normalised load	$v_p = V/V_{u,p}$	$h_p = H/H_{u,p}$	$m_p = M/M_{u,p}$
Deterministic dimensionless capacity	$V_{u,det}/Bs_{u0}$	$H_{u,det}/Bs_{u0}$	$M_{u,det}/B^2s_{u0}$
Normalised capacity	$v_u = V_{u,ran}/V_{u,det}$	$h_u = H_{u,ran}/H_{u,det}$	$m_u = M_{u,ran}/M_{u,det}$
Quantile of normalised capacity	$v_{u,p} = V_{u,p}/V_{u,det}$	$h_{u,p} = H_{u,p}/H_{u,det}$	$m_{u,p} = M_{u,p}/M_{u,det}$
Mean of normalised capacity	μ_{vu}	μ_{hu}	μ_{mu}
Coefficient of variation of normalised capacity	COV_{vu}	COV_{hu}	COV_{mu}

4. The SPCE/GSA method

4.1. The polynomial chaos expansion (PCE) method

The polynomial chaos expansion (PCE) method aims to build an analytical surrogate model to predict the response of an original model (e.g., the lower bound FE model in this study). The

system response Y can be expressed as an analytical function with regard to L independent standard random variables $\boldsymbol{\zeta} = (\zeta_1, \zeta_2, \ldots, \zeta_L)^{\mathrm{T}}$ that are used to realise random fields.

$$Y = \Gamma(\boldsymbol{\zeta}) \cong \sum_{\boldsymbol{\alpha} \in \boldsymbol{A}} k_{\boldsymbol{\alpha}} \Psi_{\boldsymbol{\alpha}}(\boldsymbol{\zeta}) \tag{8}$$

where $\Psi_{\boldsymbol{\alpha}}(\boldsymbol{\zeta})$ are the multivariate polynomials, $k_{\boldsymbol{\alpha}}$ are the corresponding unknown coefficients and the subscript $\boldsymbol{\alpha}$ is the L (i.e., the number of random variables) dimensional index. The index $\boldsymbol{\alpha} = (\alpha_1, \alpha_2, \ldots, \alpha_L)$ is an element of the index set $\boldsymbol{A} = \{\boldsymbol{\alpha}_1, \boldsymbol{\alpha}_2, \ldots, \boldsymbol{\alpha}_P\}$, where P is the total number of elements in set $\boldsymbol{A}$ and hence the number of the PCE terms. The $\Psi_{\boldsymbol{\alpha}}(\boldsymbol{\zeta})$ can be constructed by the univariate Hermite polynomial, a detailed example of which can be found in Al-Bittar and Soubra (2014).

A non-intrusive regression method is employed in this study to solve the unknown coefficients of the PCE (Sudret, 2008). Consider a matrix of N realizations $[\boldsymbol{\zeta}^{(1)}, \boldsymbol{\zeta}^{(2)}, \ldots, \boldsymbol{\zeta}^{(i)}, \ldots, \boldsymbol{\zeta}^{(N)}]^{\mathrm{T}}$ of the standard normal random vector $\boldsymbol{\zeta}^{(i)} = (\zeta_1^{(i)}, \zeta_2^{(i)}, \ldots, \zeta_L^{(i)})$ and the corresponding N realizations of FE model response $\boldsymbol{Y}' = [Y_1', Y_2', \ldots, Y_N']^{\mathrm{T}}$. The unknown coefficients can be estimated using the following equation:

$$\boldsymbol{k}' = (\boldsymbol{\Phi}^{\mathrm{T}}\boldsymbol{\Phi})^{-1}\boldsymbol{\Phi}^{\mathrm{T}}\boldsymbol{Y}' \tag{9}$$

where $\boldsymbol{k}' = [k_1', k_2', \ldots, k_P']^{\mathrm{T}}$ is the column vector of the unknown coefficients of PCE. $\boldsymbol{\Phi}$ is a $N \times P$ matrix, where an element of matrix $\Phi_{\mathrm{ij}} = \Psi_j(\boldsymbol{\zeta}^{(i)})$, $i = 1, \ldots, N$, $j = 1, \ldots, P$. The size N of realisations must be large enough to ensure a well-conditioned matrix $\boldsymbol{\Phi}^{\mathrm{T}}\boldsymbol{\Phi}$.

4.2. Sparse polynomial chaos expansion (SPCE)

Given the observation that the effect of some PCE terms on the system response is negligible (Blatman & Sudret, 2010), several techniques have been proposed for sparse polynomial chaos expansion (SPCE). A stepwise regression technique (Blatman & Sudret, 2010), least angle

regression technique (Blatman & Sudret, 2011), weighted ℓ1-minimization approach (Peng *et al.*, 2014) and Bayesian regression technique (Pan *et al.* 2020), have been successfully proposed to identify and discard the insignificant terms in order to achieve a sparse and accurate representation of PCE. In this paper, the stepwise regression technique proposed by Blatman & Sudret (2010) is adopted and briefly introduced as follows:

1) Generate N realisations of the standard normal random vector $[\boldsymbol{\zeta}^{(1)}, \boldsymbol{\zeta}^{(2)}, \ldots, \boldsymbol{\zeta}^{(N)}]^{\mathrm{T}}$ and calculate corresponding FE model responses $\boldsymbol{Y'} = [Y_1', Y_2', \ldots, Y_N']^{\mathrm{T}}$.

2) Determine user-defined parameters for the procedure, such as the target accuracy of coefficient of determination R^2_{tgt}, the maximum PCE order $n_{\max}$ and the cut-off value $\varepsilon_{\mathrm{cut}}$. In this study, these parameters are initialised as follows: $R^2_{\mathrm{tgt}} = 0.98$, $n_{\max} = 5$, $\varepsilon_{\mathrm{cut}} = 5 \times 10^{-5}$.

3) Initialise the PCE order: $n = 0$.

4) For n increasing from 1 to $n_{\max}$, the stepwise algorithm contains a forward and backward step. In the forward step, those candidate terms $\Psi_j(\boldsymbol{\zeta})$ that cause a significant increase in coefficient of determination R^2 (i.e., greater than $\varepsilon_{\mathrm{cut}}$) are identified and retained. In the backward step, the algorithm checks each term retained from $n = 1$ one by one and discards those terms that result in an insignificant decrease in R^2 (i.e., smaller than $\varepsilon_{\mathrm{cut}}$). The iteration terminates when the target accuracy is achieved or the PCE order n reaches $n_{\max}$. If the matrix $\boldsymbol{\Phi}^{\mathrm{T}}\boldsymbol{\Phi}$ is not well conditioned during this procedure, samples need to be enriched (i.e., increase N value).

For more detail on how to build up an SPCE procedure, readers may refer to Blatman & Sudret (2010) and Al-Bittar & Soubra (2013).

4.3. Global sensitivity analysis (GSA)

Global sensitivity analysis (GSA) is used to quantify the respective effects of input random variables on the variance of the system response (Sudret, 2008). The Sobol indices based GSA can be performed with the post-processing of SPCE coefficients. The first-order Sobol index $S(\zeta_i)$ for a single variable ζ_i (i = 1, …, L) can be calculated as (Sudret, 2008):

$$S\left(\zeta_i\right)=\frac{\sum_{\alpha\in\boldsymbol{A}_i^{\mathrm{T}}}\left(k_\alpha\right)^2 E\left[\left(\Psi_\alpha\right)^2\right]}{\sum_{\alpha\in\boldsymbol{A}^{\mathrm{T}}}\left(k_\alpha\right)^2 E\left[\left(\Psi_\alpha\right)^2\right]} \tag{10}$$

where k_α and Ψ_α follow definitions in Eq. (8). $\boldsymbol{A}^{\mathrm{T}}$ is the truncated index set after the SPCE procedure. $\boldsymbol{A_i}^{\mathrm{T}}$ is a subset of $\boldsymbol{A}^{\mathrm{T}}$, consisting of all indices $\boldsymbol{\alpha}$ those make $\Psi_{\boldsymbol{\alpha}}$ being single-variable functions of the random variable ζ_i. $E[(\Psi_{\boldsymbol{\alpha}})^2]$ is the expectation of $(\Psi_{\boldsymbol{\alpha}})^2$. An example of the calculation of Sobol indices based on SPCE coefficients can be found in Al-Bittar and Soubra (2014).

4.4. The SPCE/GSA procedure

In order to further improve the efficiency of SPCE, Al-Bittar and Soubra (2014) proposed the Sparse polynomial chaos expansion/Global sensitivity analysis (SPCE/GSA) procedure based on Sudret work (Sudret, 2008). The motivation of SPCE/GSA is based on the fact that random variables ζ_i (i = 1, …, L) have different contributions in the system response. Therefore, discarding random variables that have a minor influence on the system response can reduce the dimension. With the reduced dimension, a higher SPCE order can be achieved to improve the fit accuracy.

The GSA is used to calculate the weight of each random variable in the variability of system response and identify significant random variables. Typically, the GSA is conducted using a small order SPCE (e.g., n = 2) since the SPCE order has negligible influence on the Sobol

indices (Sudret, 2008; Al-Bittar & Soubra, 2014). Selection of significant input random variables includes two steps (Guo *et al.*, 2019). Firstly, variables are sorted in descending order according to corresponding Sobol indices. Then, variables with L' ($L' < L$) largest Sobol indices are selected only if the sum of L' selected Sobol indices is larger than a threshold, taken as 0.99 in this paper. The procedure of SPCE/GSA is briefly summarised below.

1) Build a 2-order SPCE with the input random variables used to generate random fields.

2) Calculate the Sobol index for each input variable with Eq. (10) and select significant input random variables according to corresponding Sobol indices.

3) Create an SPCE surrogate model with a higher order by selected significant variables.

4) Conduct Monte Carlo (MC) simulations based on the SPCE/GSA surrogate model. In the study presented in this paper, 100,000 MC simulations were conducted to obtain statistics of system responses.

5. Results

5.1. Deterministic analysis

5.1.1. Validation

Theoretically, exact solutions for uniaxial ultimate capacities fall between solutions derived from lower bound (LB) and upper bound (UB) methods. In order to validate the LB uniaxial capacities, published analytical solutions (Martin 2003) and UB solutions obtained from OPTUM G2 using the same mesh strategy as the LB are provided in Table 2. The LB solutions for vertical capacities show very good agreement with published analytical solutions derived from the method of characteristics (MoC) (Martin 2003) with a maximum difference of 2.2%. The maximum difference between LB and UB vertical capacities is 5.4%. If a finer mesh is adopted for the UB analyses, the difference can be further reduced. The dimensionless

horizontal capacity factor, H_u/Bs_{u0}, for a surface foundation is theoretically equal to unity and LB solutions are identical to exact solutions. Comparison of LB solutions for moment capacities to the available UB solutions suggests that the maximum error between LB and UB solutions is not more than 3.4%. Good agreement between LB solutions with available analytical solutions reflects the very good accuracy of LB solutions for uniaxial ultimate capacities.

Table 2 Comparison of dimensionless uniaxial capacities predicted in this study with published and exact solutions

Deterministic dimensionless capacity		$\kappa = kB/s_{u0}$			
		0	2	6	10
Vertical ($V_{u,det}/Bs_{u0}$)	This study (LB)	5.08	7.44	10.26	12.47
	This study (UB)	5.21 (2.6[a])	7.72 (3.8)	10.69 (4.2)	13.14 (5.4)
	Martin (2003) (MoC)	5.14 (1.2)	7.60 (2.2)	10.42 (1.6)	12.66 (1.5)
Horizontal ($H_{u,det}/Bs_{u0}$)	This study (LB)	1.00	1.00	1.00	1.00
	Exact solution	1.00	1.00	1.00	1.00
Moment ($M_{u,det}/B^2s_{u0}$)	This study (LB)	0.69	0.96	1.40	1.76
	This study (UB)	0.70 (1.4)	0.98 (2.1)	1.44 (2.9)	1.82 (3.4)
	Gourvenec & Randolph (2003) (UB)	0.69 (0)	0.96 (0)	1.43 (2.1)	1.86 (5.7)

Notes: [a]Percentage difference with LB solutions

Fig. 7 compares failure envelopes from the LB method to those from the UB method and the finite element method (FEM) in dimensionless loading spaces. Good agreement can be observed among failure envelopes derived from these three methods. Initially, H-M failure envelopes based on the UB method show a discrepancy with those based on LB and FE methods in some regions, as shown in Fig. 7c. With the adoption of a fine mesh in the UB analysis, the accuracy of UB solutions is improved. Good agreement between LB solutions and available analytical and FE solutions in both uniaxial capacities and failure envelopes validates the accuracy of the LB numerical model.

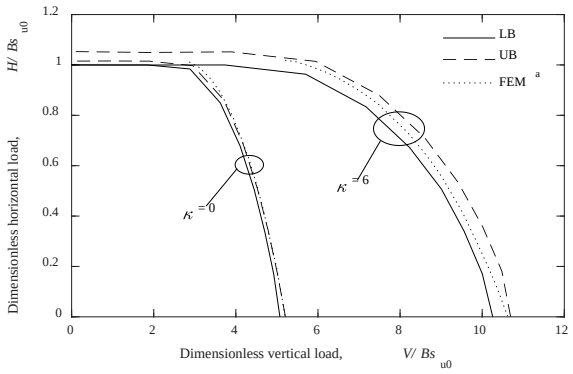

(a) V-H failure envelopes

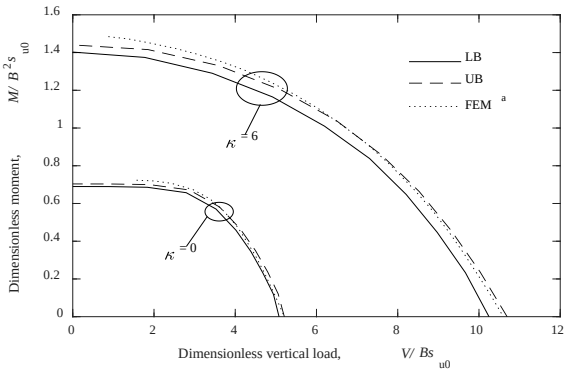

(b) V-M failure envelopes

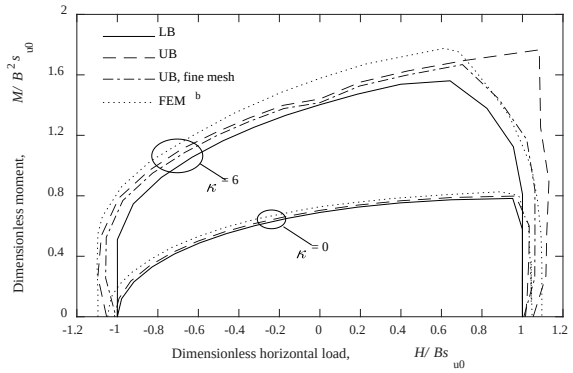

(c) H-M failure envelopes

Fig. 7. Validation of dimensionless failure envelopes in the deterministic analysis ([a]Gourvenec & Randolph, 2003; [b]Gourvenec & Barnett, 2011)

5.1.2. Approximating expressions to describe deterministic failure envelopes

Feng *et al.* (2017) and Shen *et al.* (2017a) found the form of $h = [1 - (2v - 1)^{\gamma}]^{2/3}$ is capable of describing normalised V-H failure envelopes for rectangular and circular foundations, where $h = H/H_{u,det}$, $v = V/V_{u,det}$ and γ is an exponent dependent on foundation geometry and soil strength heterogeneity index κ. In this study, normalised V-H failure envelopes for strip foundations can also be described with this form of expression as

$$h = [1 - (2v - 1)^{1.6}]^{2/3} \quad (11)$$

The normalised V-M failure envelopes contract inwards with the increasing soil heterogeneity index κ and can be well expressed with a simple power law function (Gourvenec & Randolph, 2003)

$$v = (1 - m)^{\lambda} \quad (12)$$

where λ is a function of soil strength heterogeneity index κ and can be fitted with $\lambda = 0.21 + 0.049\kappa - 0.0024\kappa^2$ in this study, which ranges from 0.21 to 0.46 when κ increases from 0 to 10, consistent with the range of 0.23 to 0.43 reported by Gourvenec & Randolph (2003) for strip foundations.

Existing expressions that describe normalised H-M failure envelopes for rectangular and circular foundations (Feng *et al.*, 2017; Shen *et al.*, 2017a) can also be employed here to fit failure envelopes for strip foundations, expressed as

$$m^q(1 - ah) + h^2 = 1 \tag{13}$$

where parameters q and a are functions of soil heterogeneity index κ and can be determined by Eqs. (14) and (15) respectively.

$$q = 2.5 + 0.16\kappa \tag{14}$$

$$a = 0.9 - 0.02\kappa \tag{15}$$

The fitting quality of Eqs. (11), (12) and (13) for normalised V-H, V-M and H-M failure envelopes are shown in Fig. 8. It can be seen that proposed equations can reasonably describe normalised failure envelopes in all loading spaces.

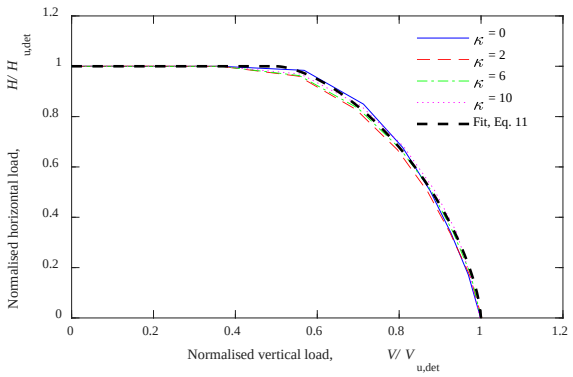

(a) V-H failure envelopes

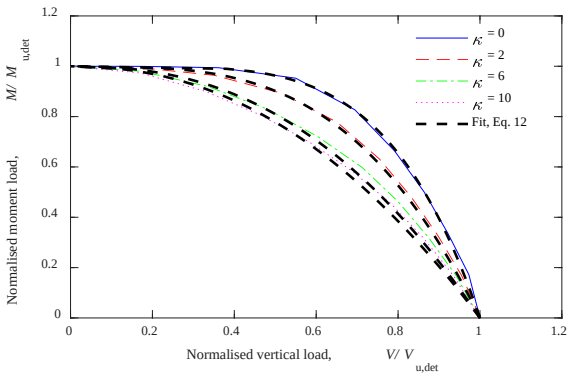

(b) V-M failure envelopes

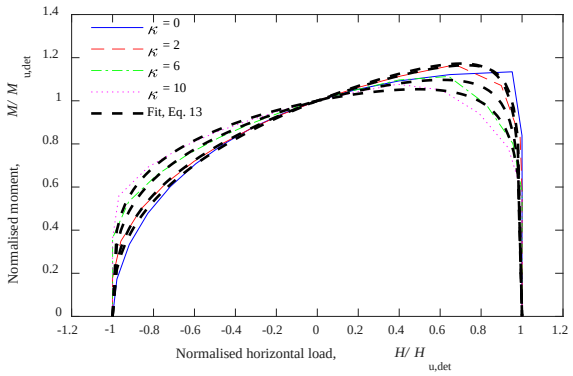

(c) H-M failure envelopes

Fig. 8. Normalised failure envelopes from deterministic analysis

5.2. Probabilistic analysis

5.2.1. Validation of SPCE/GSA method

The adopted SPCE/GSA method is validated in Fig. 9 by the comparison of RFELA results and corresponding SPCE/GSA prediction and the comparison of CDF curves constructed by classic and SPCE/GSA based MC simulations. The number of random variables for the generation of the random field mainly depends on the autocorrelation distance δ (or scale of fluctuation θ) and the finite element mesh, which decides the dimensionality of SPCE. For the case shown in Fig. 9, a total of 23 independent random variables were used to generate one random field. According to the GSA, only the most important 15 random variables were selected to construct the surrogate model. The accuracy of SPCE/GSA based surrogate model is related to the number of RFELA used for its construction. With 300 realisations of RFELA, the coefficient of determination R^2 = 0.96 was achieved for classical SPCE with the input of 23 random variables, while a higher R^2 = 0.99 was achieved for SPCE/GSA with the input of 15 random variables, as shown in Fig. 9a.

The accuracy and calculation efficiency of SPCE/GSA based MC simulation is illustrated in Fig. 9b. For SPCE/GSA based MC simulation, 300 realisations of RFELA are used to construct the CDF curve of normalised vertical capacity v_u. According to Cassidy et al. (2013), 1000 realisations of RFELA is necessary for classical MC simulation to achieve a 99% confidence

level for the accuracy of the quantile of normalised vertical capacity $v_{u,p}$ ($1\% \leqslant p \leqslant 99\%$). A classical MC simulation with 3000 realisations of RFELA is used to validate the SPCE/GSA based one. It can be seen from Fig. 9b that CDF curves constructed by two MC simulations agree very well with each other. The benefit of the SPCE/GSA technique is obvious, which considerably improve the calculation efficiency.

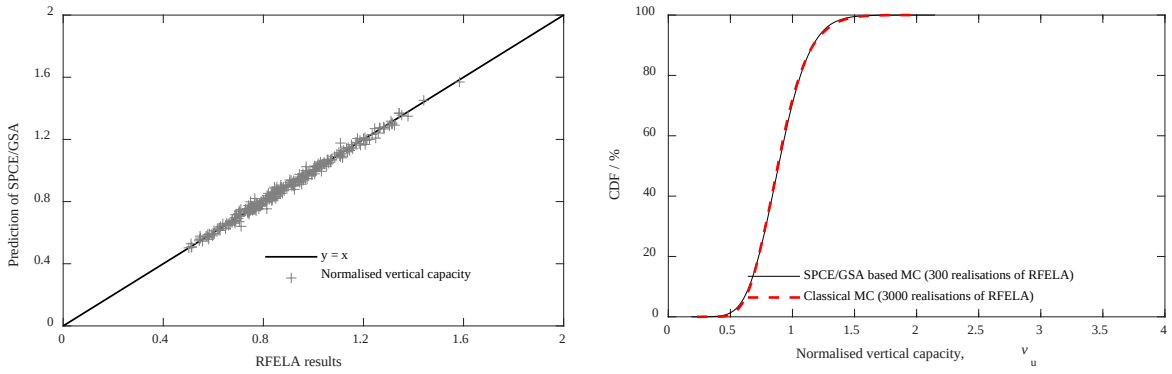

(a) comparison of RFELA results and corresponding SPCE prediction (300 realisations, $R^2 = 0.99$)

(b) comparison of CDF curves constructed by classic and SPCE/GSA based MC simulations

Fig. 9. Validation of SPCE/GSA method ($COV_{su} = 0.3$, $\kappa = 0$)

5.2.2. Uniaxial capacity

Fig. 10 shows cumulative distribution function (CDF) curves of normalised vertical capacities v_u for varying soil strength heterogeneity index κ and coefficient of variation of undrained shear strength COV_{su}. As expected, the shape of CDF curves of v_u varies with varying COV_{su} since the variation of realisations of the random field $\boldsymbol{G}_{\mathbf{su}}$ depends on COV_{su}. The CDF curves become shallower with increasing COV_{su}, reflecting the higher variation of v_u with a higher COV_{su}. For a high COV_{su}, the CDF curve at $\kappa = 0$ is set apart from those at $\kappa > 0$, consistent with previous results obtained from FEA reported by the authors (Shen *et al.*, 2020).

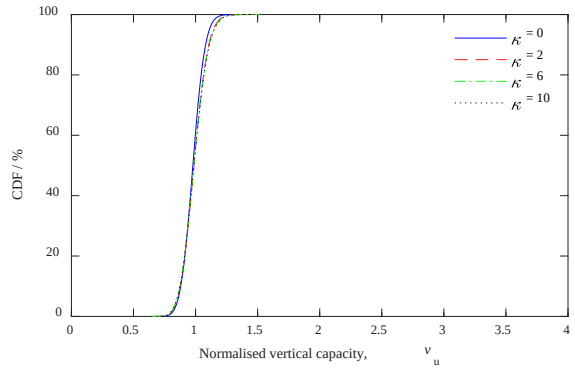

(a) COV_{su} = 0.1

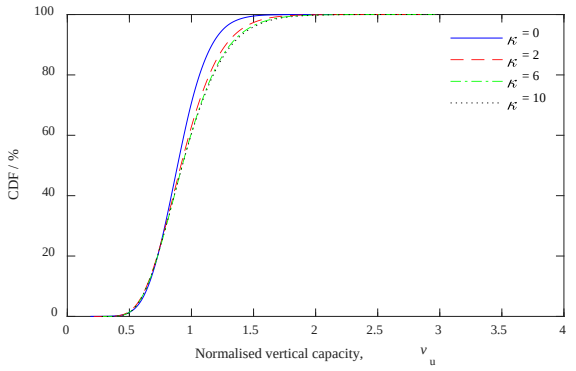

(b) COV_{su} = 0.3

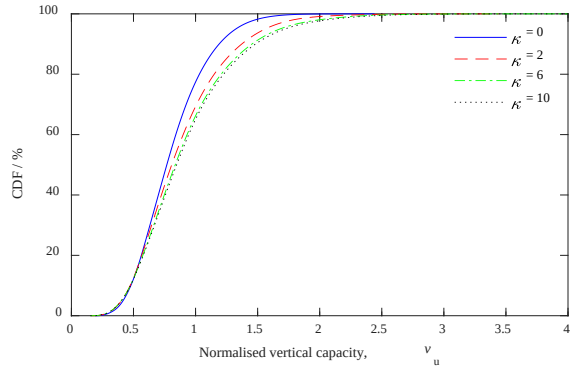

(c) COV_{su} = 0.5

Fig. 10. Cumulative distribution function (CDF) curves of normalised vertical capacities v_u for varying soil index κ and coefficient of variation of undrained shear strength COV_{su}

Figs. 11 and 12 show CDF curves of normalised horizontal (h_u) and moment (m_u) capacities, respectively. In contrast to CDF curves of v_u, CDF curves of h_u and m_u for all κ fall in a very tight band, reflecting the negligible effect of κ on the shape of CDF curves of h_u and m_u. The difference in failure mechanisms between the deterministic and probabilistic soil cases helps explain the difference between h_u (or m_u) and v_u in the performance of CDF curves with varying κ.

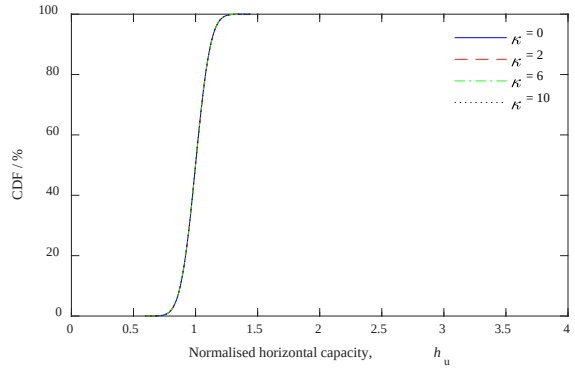

(a) COV_{su} = 0.1

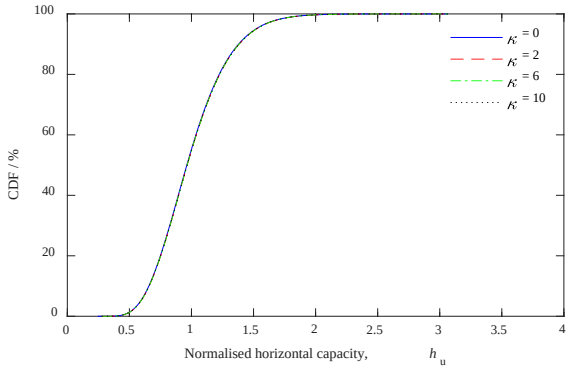

(b) COV_{su} = 0.3

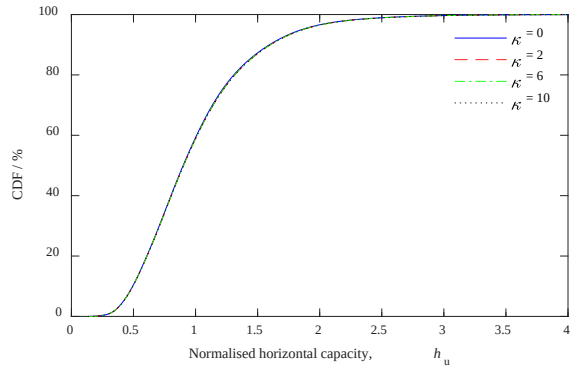

(c) COV_{su} = 0.5

Fig. 11. Cumulative distribution function (CDF) curves of normalised horizontal capacities h_u for varying soil index κ and coefficient of variation of undrained shear strength COV_{su}

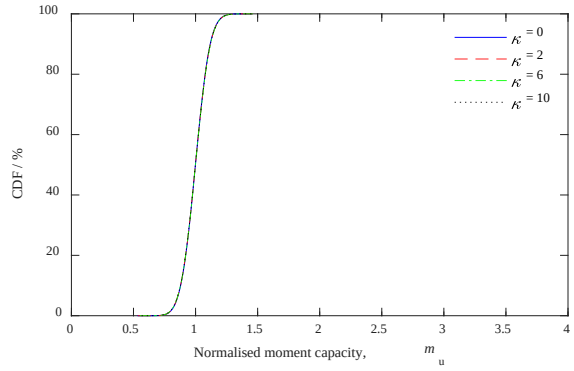

(a) COV_{su} = 0.1

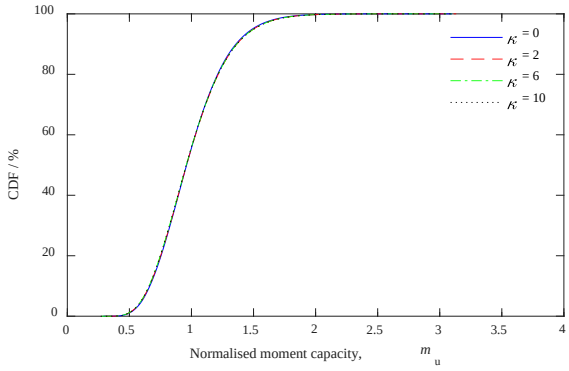

(b) COV_{su} = 0.3

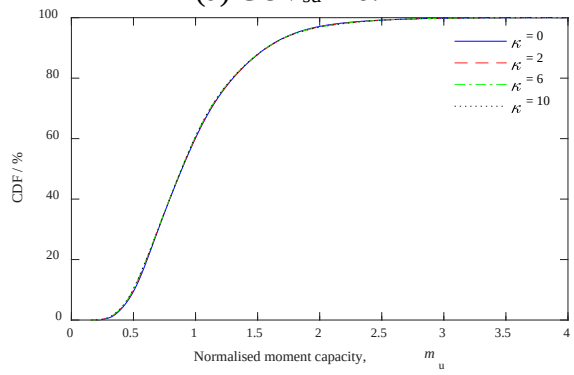

(c) COV_{su} = 0.5

Fig. 12. Cumulative distribution function (CDF) curves of normalised moment capacities m_u for varying soil index κ and coefficient of variation of undrained shear strength COV_{su}

In deterministic soil cases, failure mechanisms of surface strip foundations under horizontal loading (H) and moment (M) are base sliding and rotational scoop mechanisms (see Fig.13c) respectively, being largely independent of κ (Gourvenec & Randolph, 2003). However, for the vertical (V) loading case, the failure mechanism changes from a Prandtl type (Prandtl, 1921) (κ = 0) to a double-wedge Hill type (Hill, 1950; Kusakabe *et al.*, 1986) ($\kappa \geq 2$) as κ increases, as shown in Figs. 13a and 13b. It should be noted that the Hill type mechanism is observed for a surface circular foundation when $\kappa > 1$, irrespective of the roughness of the foundation (Kusakabe *et al.*, 1986), and the case of $\kappa = 1$ is not considered in this study. In the probabilistic

soil cases, failure mechanisms of strip foundations under *H* and *M* loadings appear to be similar to those in the deterministic analysis, which can be seen from Figs. 13c, 13g and 13h. In comparison to deterministic soil cases, failure mechanisms under *V* loading become asymmetric (see Figs. 3d and 13f) or even change to a new type of mechanism for the case of $\kappa = 0$ (see Fig. 13e) due to the soil spatial variability in probabilistic soil cases.

As such, since the sliding and rotational scoop failure mechanisms under *H* load and *M* remain similar for varying κ in deterministic and probabilistic cases, the CDF curves of h_u and m_u for all κ fall in a very tight band. By contrast, since the failure mechanism under *V* load transitions from a Prandtl mechanism (Prandtl, 1921) for $\kappa = 0$ to a double-wedge Hill mechanism (Hill, 1950) for $\kappa \geq 2$ in deterministic soil cases and becomes asymmetric or even changes to a new type in probabilistic soil cases, the CDF curves of v_u for $\kappa \geq 2$ fall in a reasonable tight band and separate to that for $\kappa = 0$ at high COV_{su}.

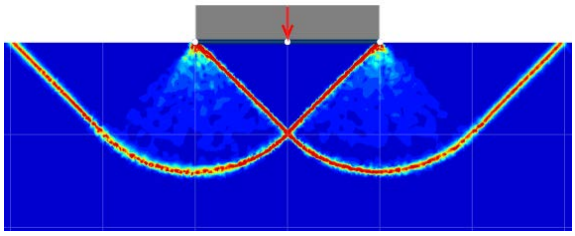

(a) deterministic: $\kappa = 0$ (Prandtl mechanism)

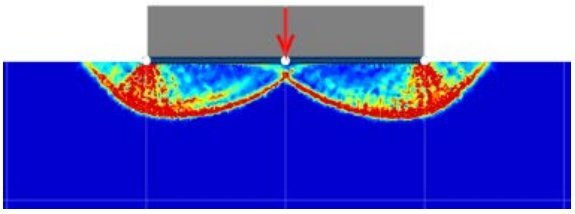

(b) deterministic: $\kappa = 10$ (Hill mechanism)

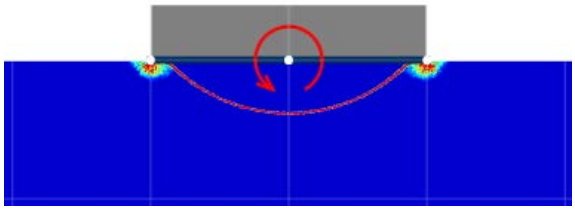

(c) deterministic: $\kappa = 10$ (scoop mechanism)

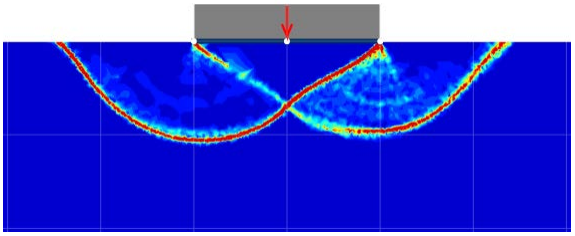

(d) probabilistic: $\kappa = 0$, $COV_{su} = 0.5$ (deformed Prandtl mechanism)

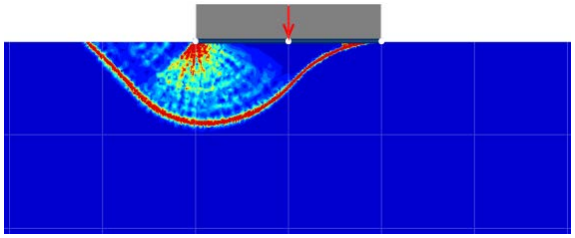

(e) probabilistic: $\kappa = 0$, $COV_{su} = 0.5$ (single-wedge mechanism)

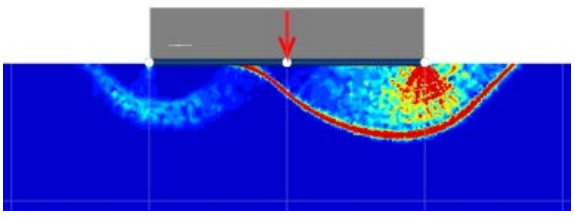

(f) probabilistic: $\kappa = 10$, $COV_{su} = 0.5$ (deformed Hill mechanism)

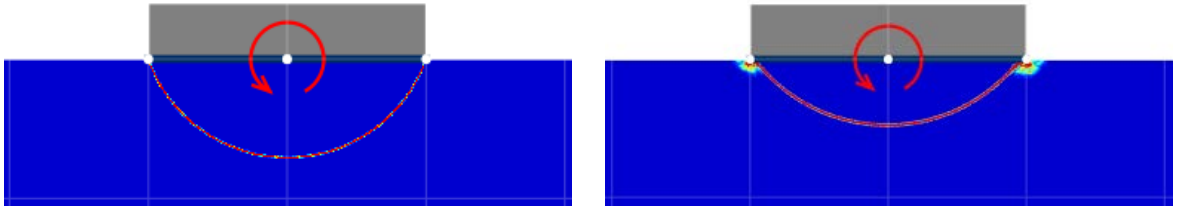

(g) probabilistic: $\kappa = 0$, $COV_{su} = 0.5$ (scoop mechanism)

(h) probabilistic: $\kappa = 10$, $COV_{su} = 0.5$ (scoop mechanism)

Fig. 13 Failure mechanisms (shown with shear dissipation band) under vertical and moment loadings for deterministic and probabilistic cases

Table 3 summarises statistics of normalised uniaxial capacities for varying combinations of κ and COV_{su}. The mean of normalised uniaxial capacities is less than or equal to unity, reflecting the spatial variation of undrained shear strength s_u reducing uniaxial capacities. The *COV* of normalised uniaxial capacities is less than the value of COV_{su} due to the spatial averaging of s_u. For example, the mix of extremely weak and strong soil zones in a numerical model would result in a reduction in the appearance of extremely low and high uniaxial capacities, which lowers the *COV* of normalised uniaxial capacities. As expected, quantiles ($1\% \leq p \leq 50\%$) of normalised uniaxial capacities decrease with the increasing COV_{su}.

The effect of dimensionless autocorrelation distance Δ on normalised uniaxial capacities is illustrated in Fig. 14. The effect of Δ on v_u appears to be more significant than that effect on h_u and m_u, which may be attributed to the different degree of variation of failure mechanisms between v_u and h_u (or m_u) in the probabilistic analysis, as stated before. The effect of Δ on capacities of shallow foundations is usually explained by limiting cases (Griffiths & Fenton, 2001; Al-Bittar & Soubra, 2013). As $\Delta \rightarrow \infty$, the shear strength s_u is nearly spatially constant in one realisation of random field $\boldsymbol{G}_{su}$ but varies among different realisations. Under this condition, the *COV*s of uniaxial capacities should be equal to the value of COV_{su}. Therefore, CDF curves of uniaxial capacities with high Δ should fall within a reasonably tight band due to matching *COV*s with one another, as shown in Fig. 14. As $\Delta \rightarrow 0$, the s_u is fully random (i.e., nearly no correlation among different locations) in each realisation of random field and weak and strong soil are fully mixed, resulting in a reduction in the appearance of extremely low and

high uniaxial capacities. This explains the cause of steeper CDF curves for low Δ as compared to the case of high Δ.

Table 3 Statistics of normalised uniaxial capacities (Δ_h = 2.5, Δ_v = 0.5)

Uniaxial capacity	COV_{su}	κ	Quantile (p = 1%)	Quantile (p = 5%)	Quantile (p = 10%)	Quantile (p = 50%)	mean	COV
v_u	0.1	0	0.804	0.854	0.880	0.979	0.980	0.080
		2	0.794	0.847	0.876	0.987	0.990	0.091
		6	0.790	0.844	0.873	0.986	0.990	0.093
		10	0.790	0.844	0.873	0.987	0.991	0.094
	0.3	0	0.483	0.591	0.651	0.888	0.900	0.224
		2	0.474	0.576	0.638	0.914	0.941	0.267
		6	0.484	0.581	0.642	0.926	0.957	0.277
		10	0.489	0.582	0.642	0.926	0.961	0.282
	0.5	0	0.310	0.416	0.479	0.768	0.802	0.333
		2	0.293	0.403	0.474	0.808	0.868	0.400
		6	0.294	0.403	0.474	0.835	0.906	0.427
		10	0.295	0.403	0.476	0.847	0.920	0.435
h_u	0.1	0	0.779	0.843	0.878	0.999	1.000	0.095
		2	0.779	0.843	0.878	1.000	1.000	0.095
		6	0.779	0.843	0.878	1.000	1.000	0.095
		10	0.779	0.843	0.878	1.000	1.000	0.095
	0.3	0	0.483	0.589	0.657	0.963	0.996	0.286
		2	0.486	0.591	0.658	0.966	0.999	0.286
		6	0.486	0.591	0.658	0.966	0.999	0.286
		10	0.486	0.591	0.658	0.966	0.999	0.286
	0.5	0	0.304	0.403	0.473	0.901	0.989	0.472
		2	0.309	0.418	0.493	0.899	0.981	0.452
		6	0.310	0.418	0.495	0.903	0.986	0.453
		10	0.310	0.418	0.495	0.903	0.986	0.453
m_u	0.1	0	0.784	0.846	0.880	0.999	0.999	0.093
		2	0.782	0.845	0.879	0.999	0.999	0.094
		6	0.782	0.844	0.879	0.999	1.000	0.094
		10	0.780	0.844	0.877	0.999	0.999	0.094
	0.3	0	0.498	0.600	0.665	0.961	0.992	0.276
		2	0.492	0.595	0.660	0.960	0.993	0.280
		6	0.490	0.593	0.658	0.959	0.991	0.282
		10	0.492	0.594	0.659	0.958	0.991	0.282
	0.5	0	0.320	0.430	0.508	0.892	0.971	0.434
		2	0.312	0.424	0.500	0.890	0.970	0.440
		6	0.307	0.420	0.496	0.885	0.966	0.442
		10	0.305	0.419	0.494	0.888	0.968	0.443

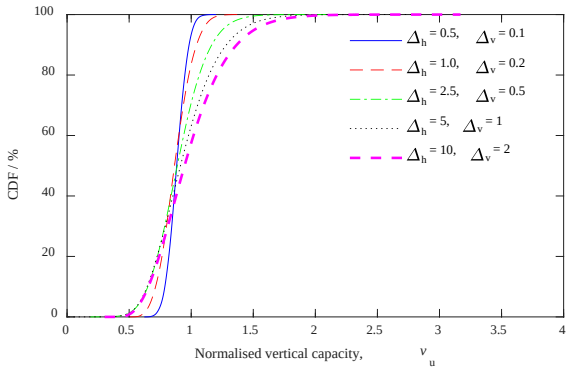

(a) vertical capacity (κ = 0)

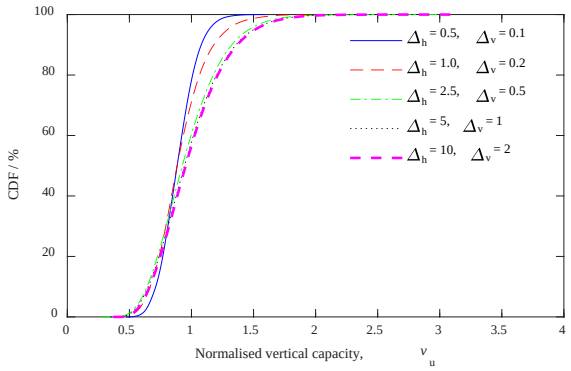

(b) vertical capacity (κ = 10)

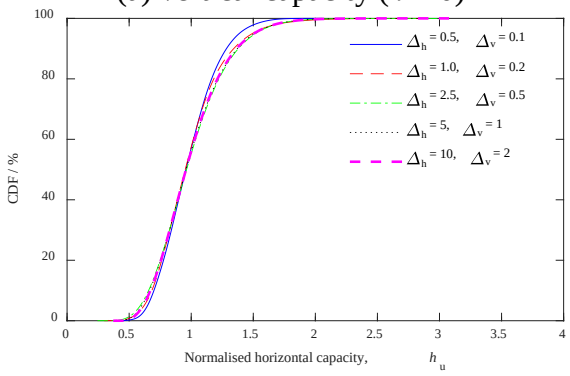

(c) horizontal capacity (κ = 0)

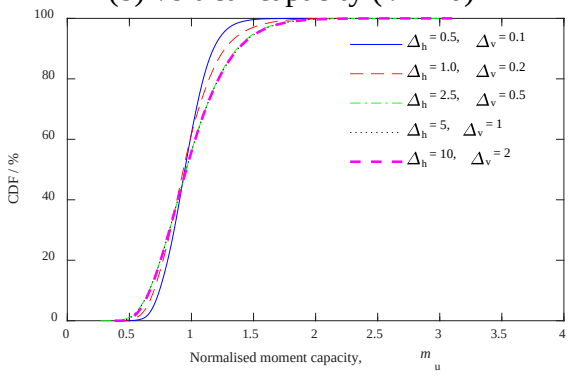

(d) moment capacity (κ = 10)

Fig. 14. Effect of dimensionless autocorrelation distance Δ on normalised uniaxial capacities (COV_{su} = 0.3)

Fig.15 presents CDF curves of normalised uniaxial capacities for 3 different autocorrelation function models (AFMs) with the same scale of fluctuation θ, including squared, single and cosine exponential AFMs. Cami et al. (2020) summarised commonly used AFMs and found these 3 AFMs covering 75% of usage. In comparison to the dimensionless autocorrelation distance Δ, the AFM has less influence on normalised uniaxial capacities. CDF curves for squared and cosine exponential AFMs fall in a tight band and are close to those curves for single exponential AFM.

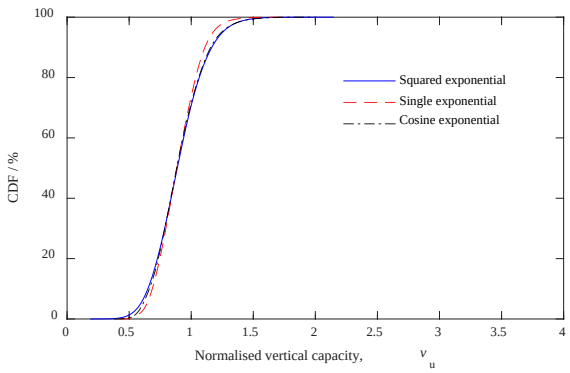

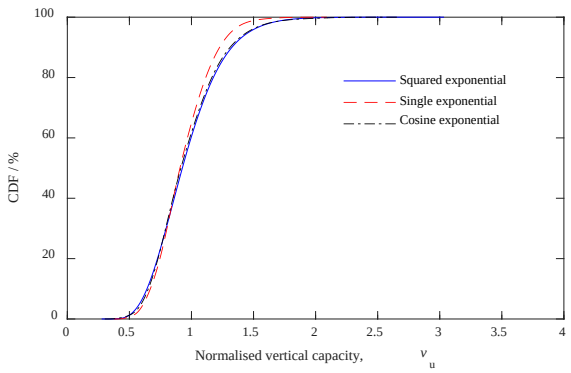

(a) vertical capacity (κ = 0) (b) vertical capacity (κ = 10)

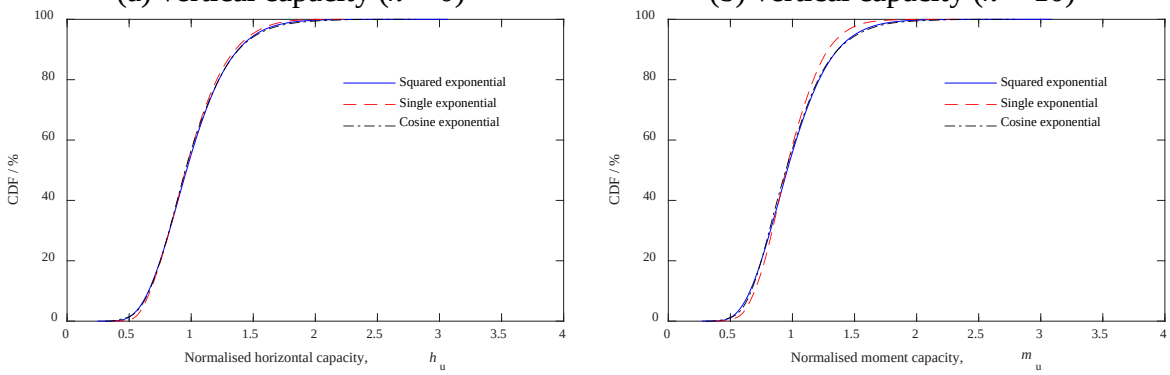

(c) horizontal capacity (κ = 0) (d) moment capacity (κ = 10)

Fig. 15. Effect of autocorrelation function model on normalised uniaxial capacities (Δ_h = 2.5, Δ_v = 0.5, COV_{su} = 0.3)

5.2.3. Probabilistic failure envelopes

The definition of probabilistic failure envelopes in this study follows that described by Charlton and Rouainia (2017). The probabilistic failure envelope corresponding to a given probability level p refers to a failure envelope consisting of a series of the quantile of failure loads $F_{u,p}$ with level p in varying loading directions. A failure load F_u in each loading direction is a random variable and its realisations are obtained through the MC simulation. For a given probability p, the quantile of failure load $F_{u,p}$ refers to the value satisfying the probability $P(F_u \leq F_{u,p}) = p$. For example, the probabilistic H-M failure envelope with p = 5% is constructed with the 5% quantile of failure loads in varying fixed loading directions in H-M loading space.

The size and shape of failure envelopes can be investigated and compared in the dimensionless and normalised loading spaces, respectively. The size of probabilistic failure envelopes has been investigated for shallow foundations on soil characterised by both stationary (Cassidy *et al.*, 2013; Hentati *et al.*, 2018) and non-stationary (Charlton & Rouainia, 2017) random fields. In this study, the shape of probabilistic failure envelopes is investigated in Figs. 16, 17 and 18 for combined V-H, V-M and H-M loadings, respectively. This is significant since capturing the change in shape of the normalised failure envelopes, enables simple scaling of a single

fitting expression by the uniaxial capacities. The deterministic uniaxial capacities $V_{u,det}$, $H_{u,det}$ and $M_{u,det}$ are used for normalising deterministic failure envelopes. For the probabilistic normalised failure envelopes at different probability level p of 1%, 5%, 10% and 50%, the probabilistic uniaxial capacities at corresponding probability level p, $V_{u,p}$, $H_{u,p}$ and $M_{u,p}$, are used for normalisation.

Fig. 16 illustrates the insignificant difference of shape between deterministic and probabilistic normalised V-H failure envelopes. Eq. (11) is proposed for deterministic V-H failure envelopes normalised by vertical and horizontal capacities $V_{u,det}$ and $H_{u,det}$. If $V_{u,det}$ and $H_{u,det}$ in Eq. (11) are replaced by $V_{u,p}$ and $H_{u,p}$, respectively, Eq. (11) can be adjusted to

$$h_p = [1 - (2v_p - 1)^{1.6}]^{2/3} \quad (16)$$

where v_p and h_p follow the definitions in Table 1 and the subscript 'p' refers to the probability level p of 1%, 5%, 10% and 50% in this study. It can be seen from Fig. 16 that Eq. (16) provides a good fit of probabilistic normalised V-H failure envelopes, the shape of which is essentially maintained at varying probability level p.

Similar to Eq. (11), Eq. (12) can be adjusted to describe the probabilistic normalised V-M failure envelopes, as

$$v_p = (1 - m_p)^{\lambda} \quad (17)$$

where the parameter λ is identical to that in Eq. (12). The fit quality of Eq. (17) can be seen in Fig. 17. Eq. (17) provides a good fit to probabilistic normalised V-M failure envelopes at a low value of $COV_{su} \leq 0.3$ across a range of soil strength heterogeneity, but slightly underestimates the envelopes as COV_{su} and κ increase. Overall, Eq. (17) provides a reasonable fit for probabilistic normalised V-M failure envelopes.

With the replacement of deterministic uniaxial capacities $H_{u,det}$ and $M_{u,det}$ by quantiles $H_{u,p}$ and $M_{u,p}$, Eq. (13) would be adjusted to

$$m_p^q(1 - ah_p) + h_p^2 = 1 \quad (18)$$

where parameters q and a can be calculated with Eqs. (14) and (15), respectively. Fig. 18 shows that probabilistic normalised H-M failure envelopes can be well described by Eq. (18) for all cases investigated in this study.

Figs. 19 and 20 illustrate the minor effect of dimensionless autocorrelation distance Δ and AFM on the shape of probabilistic normalised failure envelopes, respectively. Figs. 19 and 20 also show that the proposed Eqs. (16), (17) and (18) can be used to describe probabilistic normalised failure envelopes for a wide range of Δ and different AFMs.

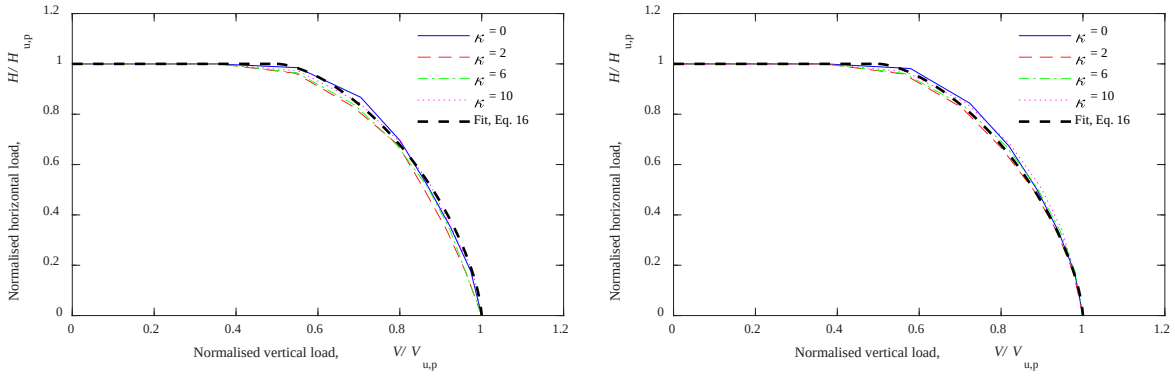

(a) COV_{su} = 0.1, p = 1% (b) COV_{su} = 0.1, p = 50%

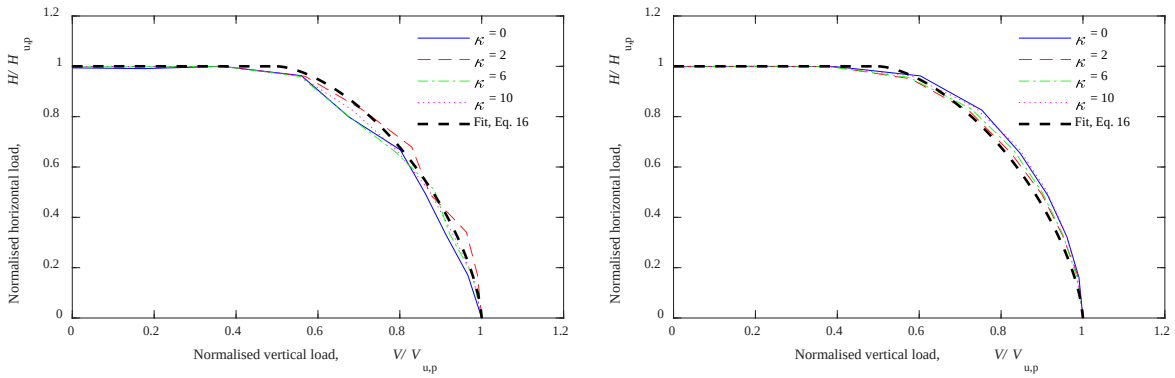

(c) COV_{su} = 0.3, p = 1% (d) COV_{su} = 0.3, p = 50%

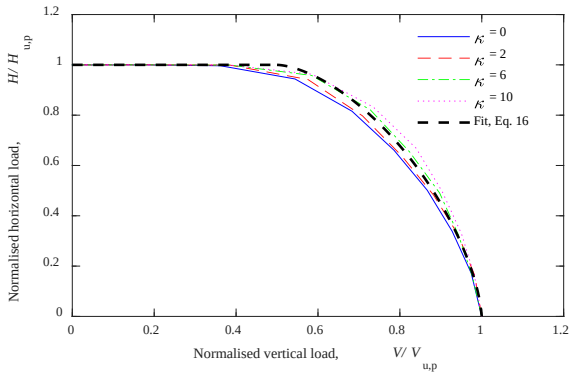

(e) COV_{su} = 0.5, p = 1%

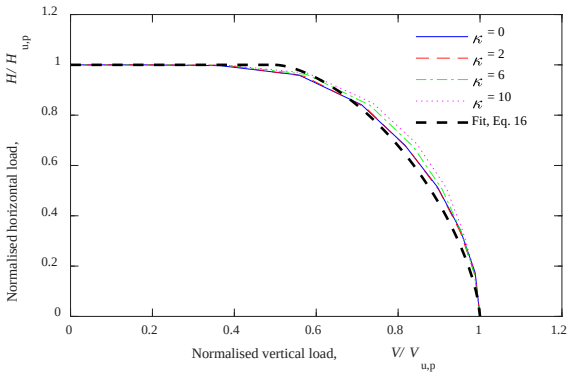

(f) COV_{su} = 0.5, p = 5%

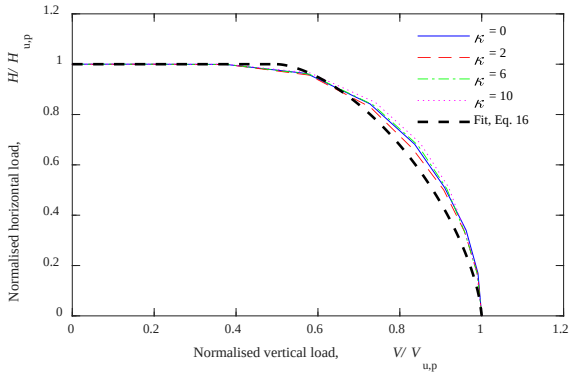

(e) COV_{su} = 0.5, p = 10%

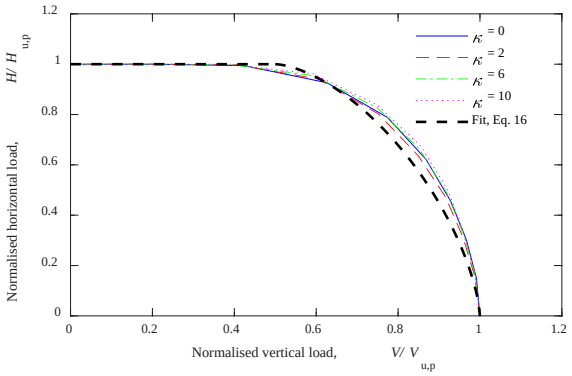

(f) COV_{su} = 0.5, p = 50%

Fig. 16. Probabilistic V-H failure envelopes

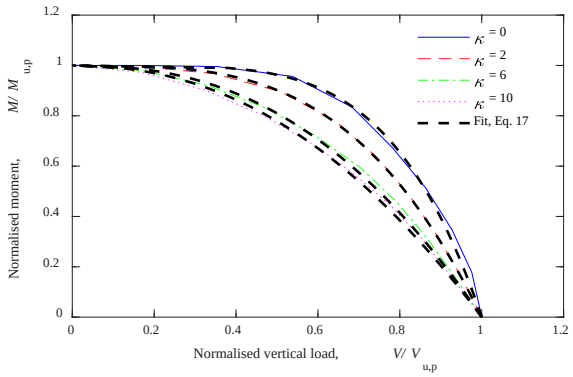

(a) COV_{su} = 0.1, p = 1%

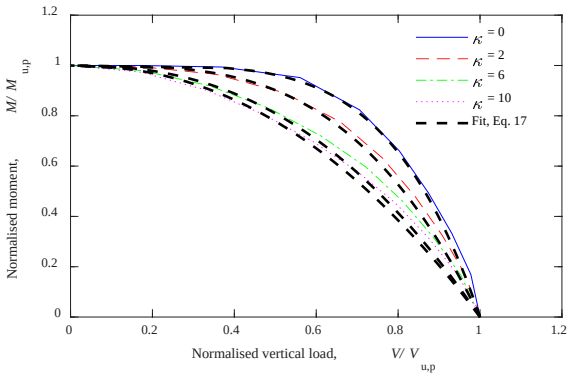

(b) COV_{su} = 0.1, p = 50%

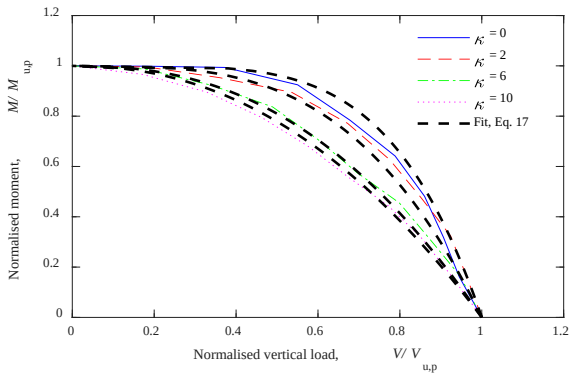

(c) COV_{su} = 0.3, p = 1%

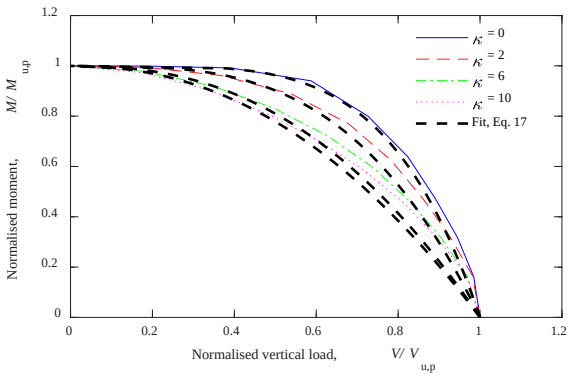

(d) COV_{su} = 0.3, p = 50%

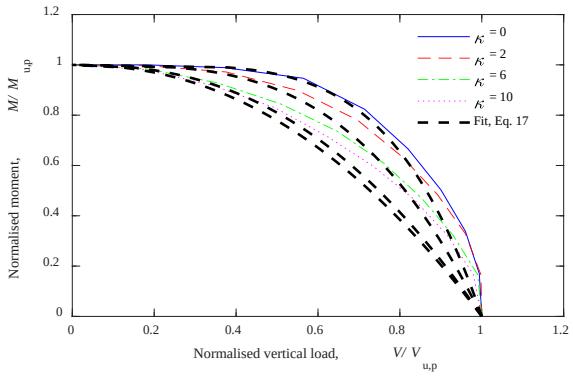

(e) COV_{su} = 0.5, p = 1%

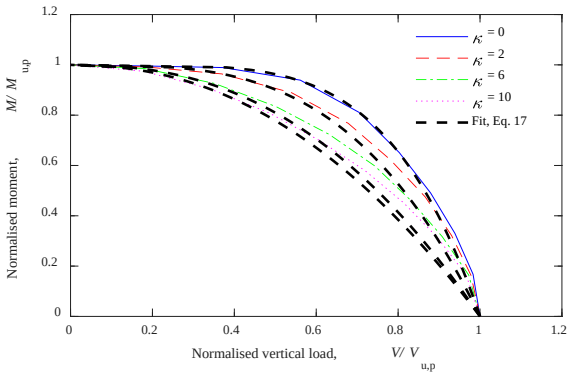

(f) COV_{su} = 0.5, p = 5%

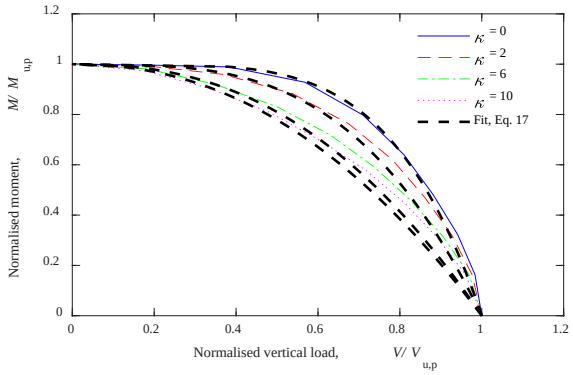

(e) COV_{su} = 0.5, p = 10%

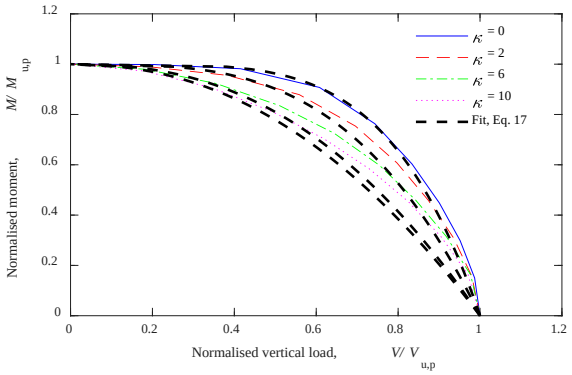

(f) COV_{su} = 0.5, p = 50%

Fig. 17. Probabilistic V-M failure envelopes

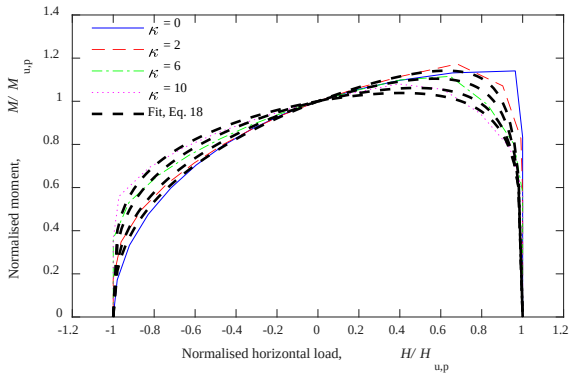

(a) COV_{su} = 0.1, p = 1%

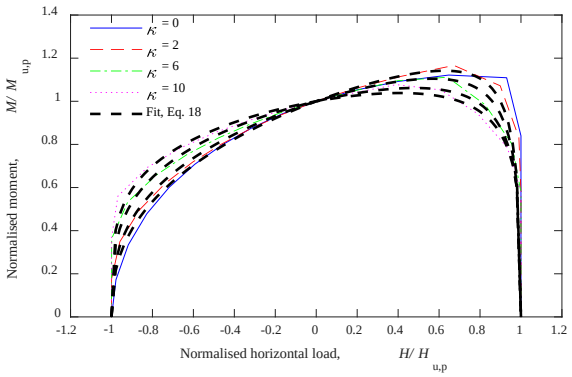

(b) COV_{su} = 0.1, p = 50%

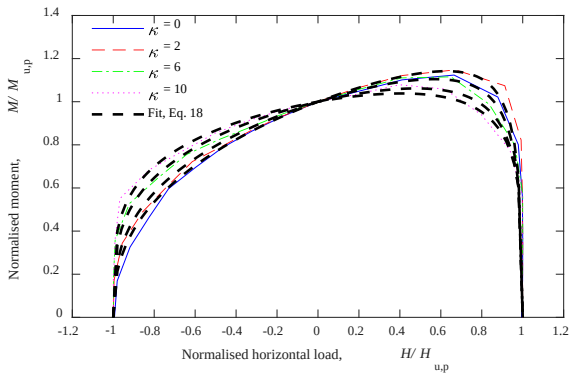

(c) COV_{su} = 0.3, p = 1%

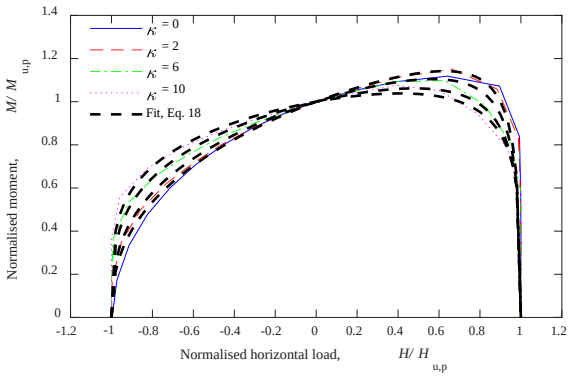

(d) COV_{su} = 0.3, p = 50%

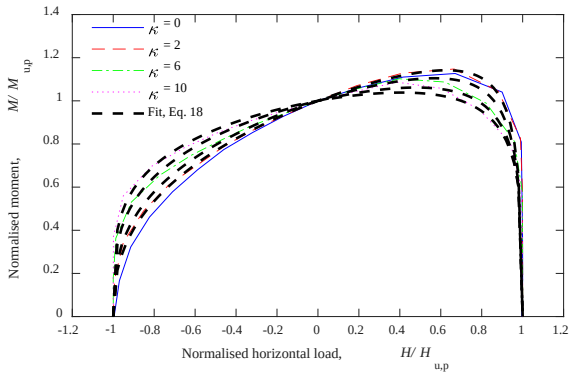

(e) COV_{su} = 0.5, p = 1%

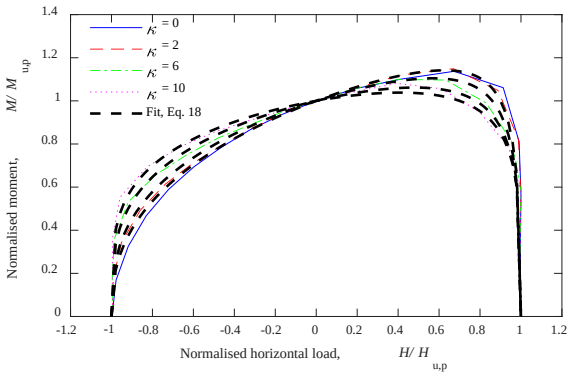

(f) COV_{su} = 0.5, p = 5%

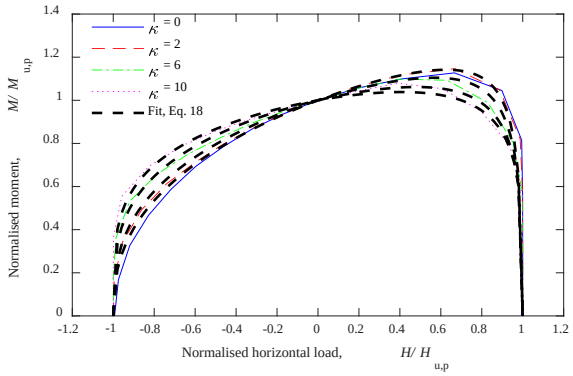

(e) COV_{su} = 0.5, p = 10%

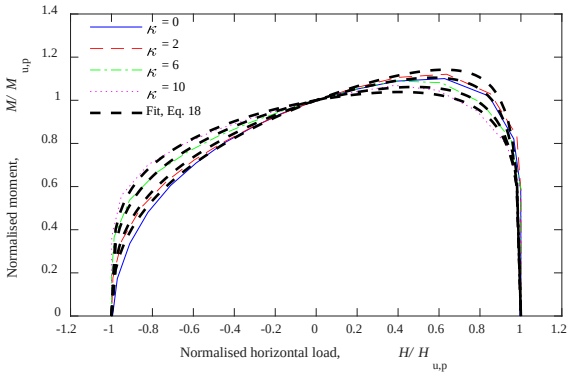

(f) COV_{su} = 0.5, p = 50%

Fig. 18. Probabilistic H-M failure envelopes

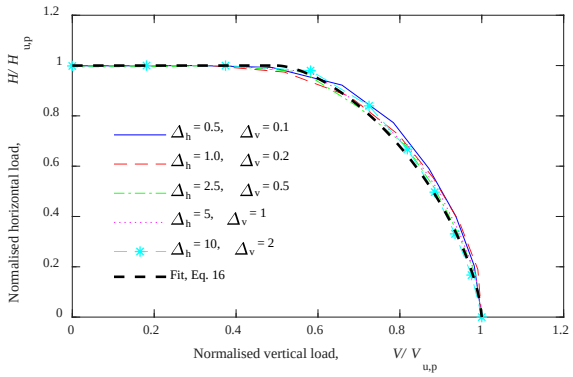

(a) V-H failure envelopes (κ = 0, p = 5%)

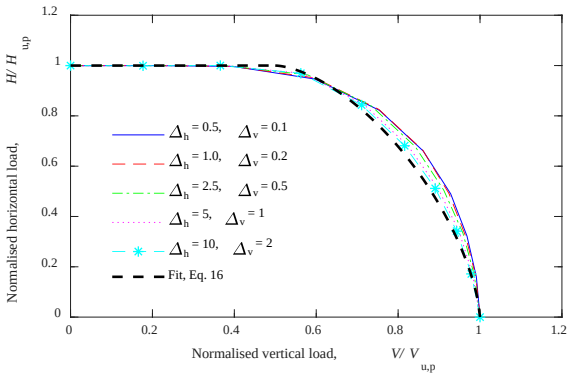

(b) V-H failure envelopes (κ = 10, p = 50%)

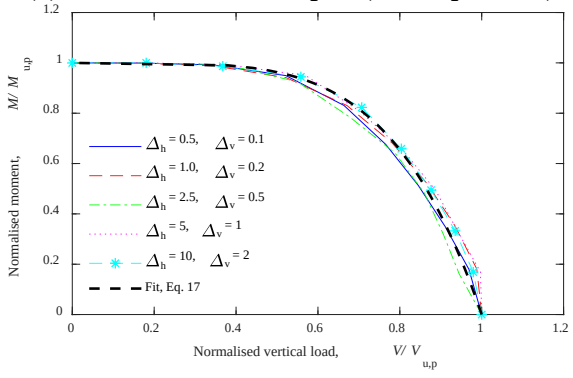

(c) V-M failure envelopes (κ = 0, p = 1%)

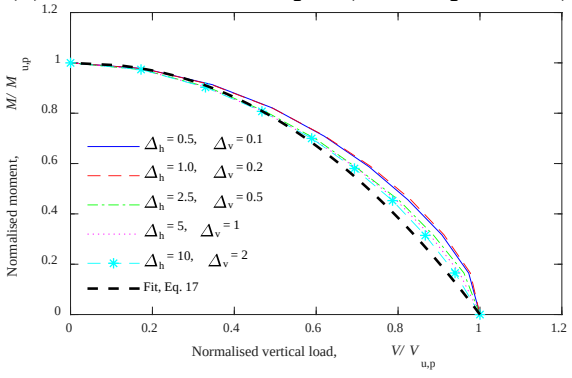

(d) V-M failure envelopes (κ = 10, p = 10%)

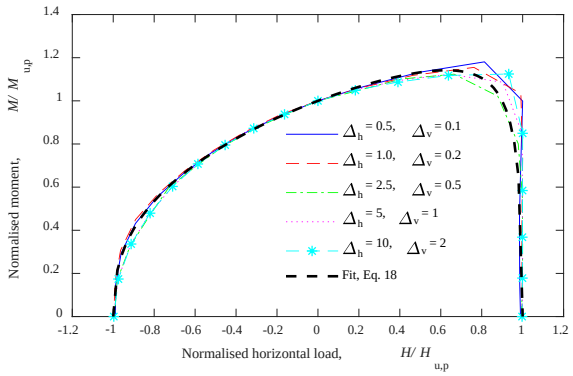

(e) H-M failure envelopes (κ = 0, p = 1%)

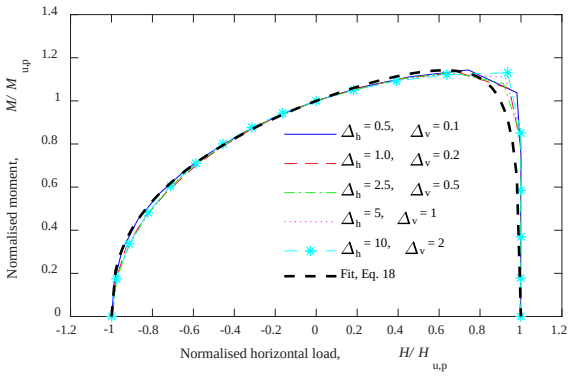

(f) H-M failure envelopes (κ = 0, p = 10%)

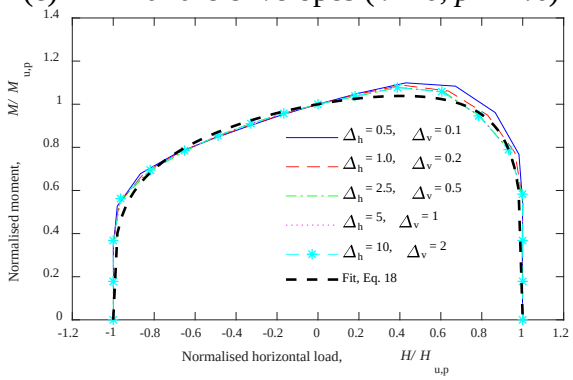

(g) H-M failure envelopes (κ = 10, p = 5%)

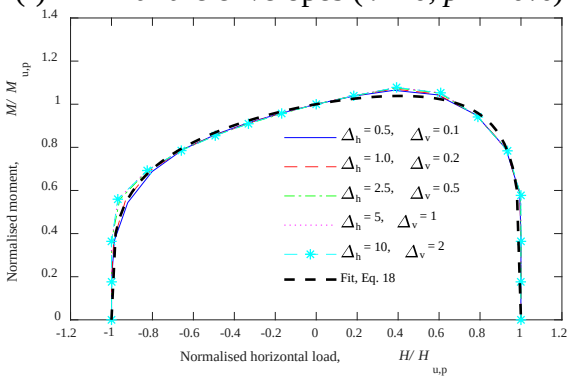

(h) H-M failure envelopes (κ = 10, p = 50%)

Fig. 19. Effect of dimensionless autocorrelation distance Δ on probabilistic failure envelopes (COV_{su} = 0.3)

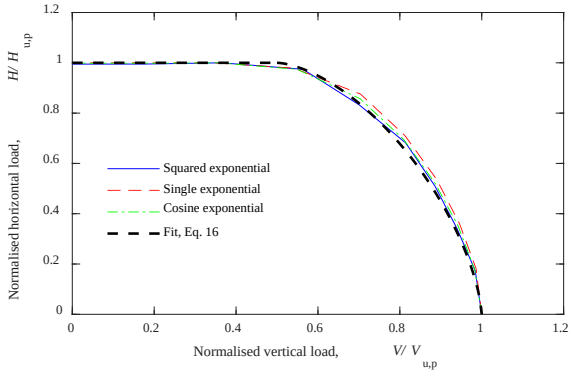

(a) V-H failure envelopes (κ = 0, p = 5%)

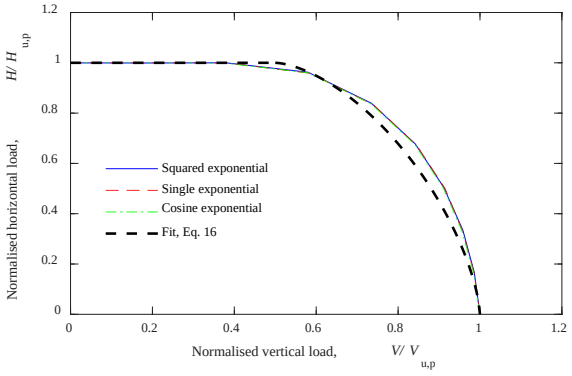

(b) V-H failure envelopes (κ = 10, p = 50%)

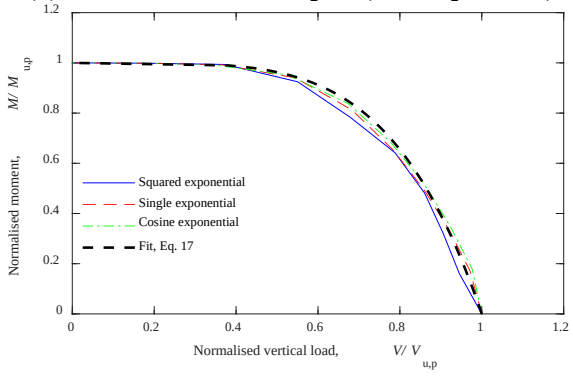

(c) V-M failure envelopes (κ = 0, p = 1%)

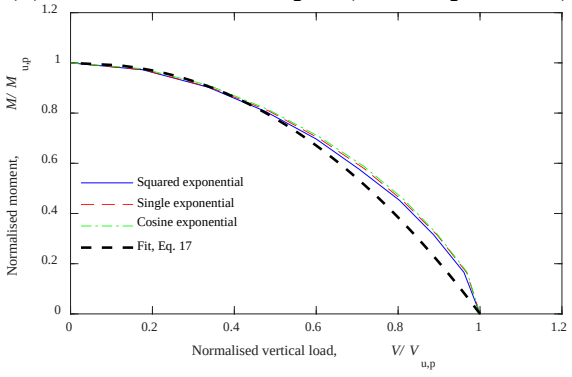

(d) V-M failure envelopes (κ = 10, p = 10%)

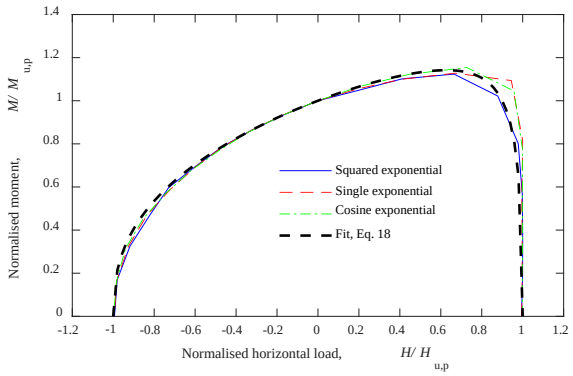

(e) H-M failure envelopes (κ = 0, p = 1%)

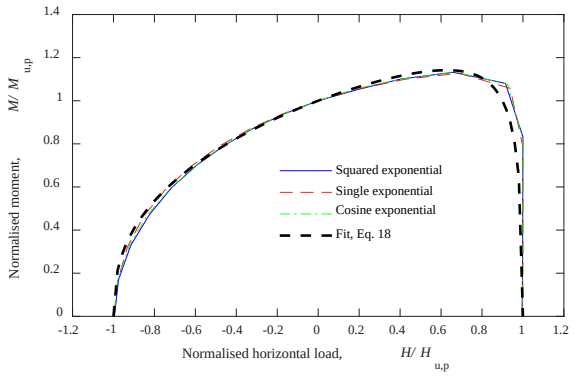

(f) H-M failure envelopes (κ = 0, p = 10%)

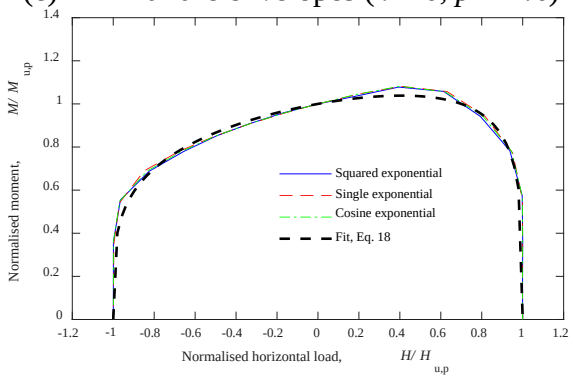

(g) H-M failure envelopes (κ = 10, p = 5%)

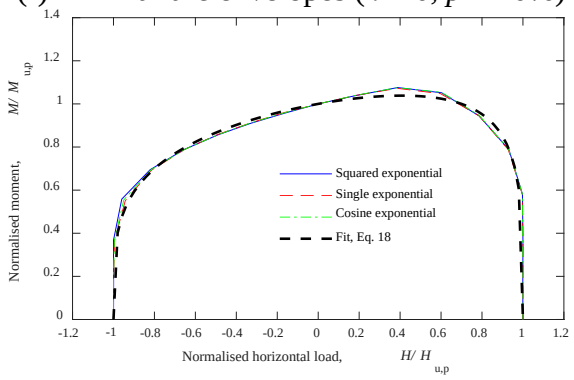

(h) H-M failure envelopes (κ = 10, p = 50%)

Fig. 20. Effect of autocorrelation function model on probabilistic failure envelopes (Δ_h = 2.5, Δ_v = 0.5, COV_{su} = 0.3)

6. Conclusions

Probabilistic failure envelopes of strip foundations under planar V-H-M loading on soil with spatially variable s_u have been investigated using lower bound random finite element limit analysis. The results of this study show that the difference in shape between deterministic and probabilistic failure envelopes is minimal and for practical purposes can be neglected. Parameters COV_{su} and Δ that are used to describe a random field $\boldsymbol{G}_{su}$ can considerably influence the probabilistic normalised uniaxial capacities and hence the size of probabilistic failure envelopes but have an insignificant effect on the shape of probabilistic failure envelopes. In contrast, the soil heterogeneity index κ has the lowest effect on probabilistic normalised uniaxial capacities in comparison to COV_{su} and Δ but has the highest effect on the shape of probabilistic failure envelopes. The autocorrelation function models have an insignificant effect on both size and shape of probabilistic failure envelopes.

The findings from this study provide a simple-to-use framework to capture V-H-M capacity of strip foundations on spatially variable soil.

Acknowledgements

This work is supported by State Key Laboratory of Hydraulic Engineering Simulation and Safety (Tianjin University). Susan Gourvenec is supported by the Royal Academy of Engineering under the Chairs in Emerging Technologies scheme. Yinghui Tian is supported by Australian Research Council Future Fellowship.

References

Al-Bittar, T. & Soubra, A.-H. (2013) Bearing capacity of strip footings on spatially random soils using sparse polynomial chaos expansion. *International Journal for Numerical and Analytical Methods in Geomechanics* **37(13)**:2039-2060. https://doi.org/10.1002/nag.2120.

Al-Bittar, T. & Soubra, A. H. (2014) Efficient sparse polynomial chaos expansion methodology for the probabilistic analysis of computationally-expensive deterministic models. *International Journal for Numerical and Analytical Methods in Geomechanics* **38(12)**:1211-1230. https://doi.org/10.1002/nag.2251.

Blatman, G. & Sudret, B. (2010) An adaptive algorithm to build up sparse polynomial chaos expansions for stochastic finite element analysis. *Probabilistic Engineering Mechanics* **25(2)**:183-197. https://doi.org/10.1016/j.probengmech.2009.10.003.

Blatman, G. & Sudret, B. (2011) Adaptive sparse polynomial chaos expansion based on least angle regression. *Journal of Computational Physics* **230(6)**:2345-2367. https://doi.org/10.1016/j.jcp.2010.12.021.

Bransby, M. F. & Randolph, M. F. (1998) Combined loading of skirted foundations. *Géotechnique* **48(5)**:637-655. https://doi.org/10.1680/geot.1998.48.5.637.

Cami, B., Javankhoshdel, S., Phoon, K.-K. & Ching, J. (2020) Scale of fluctuation for spatially varying soils: estimation methods and values. *ASCE-ASME Journal of Risk and Uncertainty in Engineering Systems, Part A: Civil Engineering* **6(4)**:03120002. https://doi.org/10.1061/AJRUA6.0001083.

Cassidy, M. J., Uzielli, M. & Tian, Y. (2013) Probabilistic combined loading failure envelopes of a strip footing on spatially variable soil. *Computers and Geotechnics* **49**:191-205. https://doi.org/10.1016/j.compgeo.2012.10.008.

Charlton, T. S. & Rouainia, M. (2017) A probabilistic approach to the ultimate capacity of skirted foundations in spatially variable clay. *Structural Safety* **65**:126-136. https://doi.org/10.1016/j.strusafe.2016.05.002.

Ching, J., Wu, S.-S. & Phoon, K.-K. (2016) Statistical characterization of random field parameters using frequentist and Bayesian approaches. *Canadian Geotechnical Journal* **53(2)**:285-298. https://doi.org/10.1139/cgj-2015-0094.

Davis, M. W. (1987) Production of conditional simulations via the LU triangular decomposition of the covariance matrix. *Mathematical Geology* **19(2)**:91-98. https://doi.org/10.1007/BF00898189.

Degroot, D. J. & Baecher, G. B. (1993) Estimating autocovariance of in-situ soil properties. *Journal of Geotechnical Engineering* **119(1)**:147-166. https://doi-org.libproxy1.nus.edu.sg/10.1061/(ASCE)0733-9410(1993)119:1(147).

Duncan, J. M. (2000) Factors of Safety and Reliability in Geotechnical Engineering. *Journal of Geotechnical and Geoenvironmental Engineering* **126(4)**:307-316. https://doi.org/10.1061/(ASCE)1090-0241(2000)126:4(307).

Feng, X., Gourvenec, S. & Shen, Z. (2017) Shape effects on undrained capacity of mudmat foundations under multi-directional loading. *Ocean Engineering* **135**:221-235. https://doi.org/10.1016/j.oceaneng.2017.02.033.

Feng, X., Randolph, M. F., Gourvenec, S. & Wallerand, R. (2014) Design approach for rectangular mudmats under fully three-dimensional loading. *Géotechnique* **64(1)**:51-63. https://doi.org/10.1680/geot.13.P.051.

Fenton, G. A. (1999) Estimation for Stochastic Soil Models. *Journal of Geotechnical and Geoenvironmental Engineering* **125(6)**:470-485. https://doi.org/10.1061/(ASCE)1090-0241(1999)125:6(470).

Gourvenec, S. (2007) Failure envelopes for offshore shallow foundations under general loading. *Géotechnique* **57(9)**:715-728. https://doi.org/10.1680/geot.2007.57.9.715.

Gourvenec, S. (2008) Effect of embedment on the undrained capacity of shallow foundations under general loading. *Géotechnique* **58(3)**:177-185. https://doi.org/10.1680/geot.2008.58.3.177.

Gourvenec, S. & Barnett, S. (2011) Undrained failure envelope for skirted foundations under general loading. *Géotechnique* **61(3)**:263-270. https://doi.org/10.1680/geot.9.T.027.

Gourvenec, S. & Randolph, M. F. (2003) Effect of strength non-homogeneity on the shape of failure envelopes for combined loading of strip and circular foundations on clay. *Géotechnique* **53(6)**:575-586. https://doi.org/10.1680/geot.2003.53.6.575.

Griffiths, D. V. & Fenton, G. A. (2001) Bearing capacity of spatially random soil: the undrained clay Prandtl problem revisited. *Géotechnique* **51(4)**:351-359. https://doi.org/10.1680/geot.2001.51.4.351.

Griffiths, D. V., Fenton, G. A. & Manoharan, N. (2002) Bearing Capacity of Rough Rigid Strip Footing on Cohesive Soil: Probabilistic Study. *Journal of Geotechnical and Geoenvironmental Engineering* **128(9)**:743-755. https://doi.org/10.1061/(ASCE)1090-0241(2002)128:9(743).

Guo, X., Dias, D. & Pan, Q. (2019) Probabilistic stability analysis of an embankment dam considering soil spatial variability. *Computers and Geotechnics* **113**:103093. https://doi.org/10.1016/j.compgeo.2019.103093.

Hentati, A., Selmi, M., Kormi, T. & Ali, N. B. H. (2018) Probabilistic HM failure envelopes of strip foundations on spatially variable soil. *Computers and Geotechnics* **102**:66-78. https://doi.org/10.1016/j.compgeo.2018.06.001.

Hill, R. (1950) *The mathematical theory of plasticity*. New York, USA: Oxford University Press.

Jha Sanjay, K. (2016) Reliability-Based Analysis of Bearing Capacity of Strip Footings Considering Anisotropic Correlation of Spatially Varying Undrained Shear Strength. *International Journal of Geomechanics* **16(5)**:06016003. https://doi.org/10.1061/(ASCE)GM.1943-5622.0000638.

Kasama, K. & Whittle, A. J. (2011) Bearing Capacity of Spatially Random Cohesive Soil Using Numerical Limit Analyses. *Journal of Geotechnical and Geoenvironmental Engineering* **137(11)**:989-996. https://doi.org/10.1061/(ASCE)GT.1943-5606.0000531.

Keaveny, J. M., Nadim, F., and Lacasse, S (1989) Autocorrelation functions for offshore geotechnical data. In *Proceedings of the 5th International Conference on Structural Safety and Reliability*.), San Francisco, pp. 263–270.

Krabbenhoft, K. (2019a) *OPTUM G2: Analysis.* Denmark: Optum Computational Engineering.

Krabbenhoft, K. (2019b) *OPTUM G2: Features.* Denmark: Optum Computational Engineering.

Krabbenhoft, K. (2019c) *OPTUM G2: Materials.* Denmark: Optum Computational Engineering.

Kusakabe, O., Suzuki, H. & Nakase, A. (1986) An Upper Bound Calculation on Bearing Capacity of a Circular Footing on a Non-Homogeneous Clay. *Soils and Foundations* **26(3)**:143-148. https://doi.org/10.3208/sandf1972.26.3_143.

Li, D.-Q., Qi, X.-H., Cao, Z.-J., Tang, X.-S., Zhou, W., Phoon, K.-K. & Zhou, C.-B. (2015) Reliability analysis of strip footing considering spatially variable undrained shear strength that linearly increases with depth. *Soils and Foundations* **55(4)**:866-880. https://doi.org/10.1016/j.sandf.2015.06.017.

Li, J. H., Zhou, Y., Zhang, L. L., Tian, Y., Cassidy, M. J. & Zhang, L. M. (2016) Random finite element method for spudcan foundations in spatially variable soils. *Engineering Geology* **205**:146-155. https://doi.org/10.1016/j.enggeo.2015.12.019.

Liu, W. F. & Leung, Y. F. (2018) Characterising three-dimensional anisotropic spatial correlation of soil properties through in situ test results. *Géotechnique* **68(9)**:805-819. https://doi.org/10.1680/jgeot.16.P.336.

Martin, C. (2003) New software for rigorous bearing capacity calculations. In *BGA International Conference on Foundations: innovations, observations, design and practice*.), Dundee, UK, pp. 581-592.

Pan, Q. & Dias, D. (2017) Probabilistic evaluation of tunnel face stability in spatially random soils using sparse polynomial chaos expansion with global sensitivity analysis. *Acta Geotechnica* **12(6)**:1415-1429. https://doi.org/10.1007/s11440-017-0541-5.

Pan, Q., Qu, X., Liu, L. & Dias, D. (2020) A sequential sparse polynomial chaos expansion using Bayesian regression for geotechnical reliability estimations. *International Journal*

for Numerical and Analytical Methods in Geomechanics **44**:874-889. https://doi.org/10.1002/nag.3044.

Peng, J., Hampton, J. & Doostan, A. (2014) A weighted ℓ1-minimization approach for sparse polynomial chaos expansions. *Journal of Computational Physics* **267**:92-111. https://doi.org/10.1016/j.jcp.2014.02.024.

Phoon, K.-K. & Kulhawy, F. H. (1999) Characterization of geotechnical variability. *Canadian Geotechnical Journal* **36(4)**:612-624. https://doi.org/10.1139/t99-038.

Phoon, K.-K., Quek, S.-T. & An, P. (2003) Identification of Statistically Homogeneous Soil Layers Using Modified Bartlett Statistics. *Journal of Geotechnical and Geoenvironmental Engineering* **129(7)**:649-659. https://doi.org/10.1061/(ASCE)1090-0241(2003)129:7(649).

Popescu, R., Deodatis, G. & Nobahar, A. (2005) Effects of random heterogeneity of soil properties on bearing capacity. *Probabilistic Engineering Mechanics* **20(4)**:324-341. https://doi.org/10.1016/j.probengmech.2005.06.003.

Prandtl, L. (1921) Hauptaufsätze: Über die Eindringungsfestigkeit (Härte) plastischer Baustoffe und die Festigkeit von Schneiden. *Zeitschrift für Angewandte Mathematik und Mechanik (Journal of Applied Mathematics and Mechanics)* **1(1)**:15-20. https://doi.org/10.1002/zamm.19210010102.

Selmi, M., Kormi, T., Hentati, A. & Ali, N. (2019) Capacity assessment of offshore skirted foundations under HM combined loading using RFEM. *Computers and Geotechnics* **114**:103148. https://doi.org/10.1016/j.compgeo.2019.103148.

Shen, Z., Bie, S. & Guo, L. (2017a) Undrained capacity of a surface circular foundation under fully three-dimensional loading. *Computers and Geotechnics* **92**:57-67. https://doi.org/10.1016/j.compgeo.2017.07.018.

Shen, Z., Feng, X. & Gourvenec, S. (2016) Undrained capacity of surface foundations with zero-tension interface under planar V-H-M loading. *Computers and Geotechnics* **73**:47-57. http://dx.doi.org/10.1016/j.compgeo.2015.11.024.

Shen, Z., Feng, X. & Gourvenec, S. (2017b) Effect of interface condition on the undrained capacity of subsea mudmats under six-degree-of-freedom loading. *Géotechnique* **67(4)**:338-349. https://doi.org/10.1680/jgeot.16.P.097.

Shen, Z., Jin, D., Pan, Q., Yang, H. & Chian, S. C. (2020) Probabilistic analysis of strip footings on spatially variable soils with linearly increasing shear strength. *Computers and Geotechnics* **126**:103653. https://doi.org/10.1016/j.compgeo.2020.103653.

Shi, G., Pan, Y., Sun, Z., Liu, Y. & Lee, F.-H. (2019) Characteristic strength of soils underlying foundations considering effect of spatial variability. *Canadian Geotechnical Journal* **57(4)**:518-536. https://doi.org/10.1139/cgj-2019-0043.

Stuedlein, A. W., Kramer, S. L., Arduino, P. & Holtz, R. D. (2012) Geotechnical Characterization and Random Field Modeling of Desiccated Clay. *Journal of Geotechnical and Geoenvironmental Engineering* **138(11)**:1301-1313. https://doi.org/10.1061/(ASCE)GT.1943-5606.0000723.

Sudret, B. (2008) Global sensitivity analysis using polynomial chaos expansions. *Reliability Engineering & System Safety* **93(7)**:964-979. https://doi.org/10.1016/j.ress.2007.04.002.

Taiebat, H. A. & Carter, J. P. (2000) Numerical studies of the bearing capacity of shallow foundations on cohesive soil subjected to combined loading. *Géotechnique* **50(4)**:409-418. https://doi.org/10.1680/geot.2000.50.4.409.

Tian, M., Li, D.-Q., Cao, Z.-J., Phoon, K.-K. & Wang, Y. (2016) Bayesian identification of random field model using indirect test data. *Engineering Geology* **210**:197-211. https://doi.org/10.1016/j.enggeo.2016.05.013.

Uzielli, M., Lacasse, S., Nadim, F. & Phoon, K. K. (2007) Soil variability analysis for geotechnical practice. In *Characterization and engineering properties of natural soils.* (Tan, T. S., Phoon, K. K., Hight, D. W., and Leroueil, S. (eds)) Taylor & Francis Group, London, vol. 3, pp. 1653-1752.

Uzielli, M., Vannucchi, G. & Phoon, K. K. (2005) Random field characterisation of stress-nomalised cone penetration testing parameters. *Géotechnique* **55(1)**:3-20. https://doi.org/10.1680/geot.2005.55.1.3.

Vanmarcke, E. H. (1983) *Random fields: analysis and synthesis.* London, UK: MIT Press.

Vulpe, C., Gourvenec, S., Leman, B. & Fung, K. N. (2016) Failure Envelope Approach for Consolidated Undrained Capacity of Shallow Foundations. *Journal of Geotechnical and Geoenvironmental Engineering* **142(8)**:04016036. https://doi.org/10.1061/(ASCE)GT.1943-5606.0001498.

Vulpe, C., Gourvenec, S. M. & Cornelius, A. F. (2017) Effect of embedment on consolidated undrained capacity of skirted circular foundations in soft clay under planar loading. *Canadian Geotechnical Journal* **54(2)**:158-172. https://doi.org/10.1139/cgj-2016-0265.

Wang, Y., Au, S.-K. & Cao, Z. (2010) Bayesian approach for probabilistic characterization of sand friction angles. *Engineering Geology* **114(3)**:354-363. https://doi.org/10.1016/j.enggeo.2010.05.013.

Xiao, T., Li, D.-Q., Cao, Z.-J. & Zhang, L.-M. (2018) CPT-based probabilistic characterization of three-dimensional spatial variability using MLE. *Journal of Geotechnical and Geoenvironmental Engineering* **144(5)**:04018023. https://doi.org/10.1061/(ASCE)GT.1943-5606.0001875.

Xiao, Z., Tian, Y. & Gourvenec, S. (2016) A practical method to evaluate failure envelopes of shallow foundations considering soil strain softening and rate effects. *Applied Ocean Research* **59**:395-407. https://doi.org/10.1016/j.apor.2016.06.015.

Yi, J. T., Pan, Y. T., Huang, L. Y., Xu, S. J., Liu, Y. & Phoon, K. K. (2020) Determination of limiting cavity depths for offshore spudcan foundations in a spatially varying seabed. *Marine Structures* **71**:102723. https://doi.org/10.1016/j.marstruc.2020.102723.

Zhang, L., Li, J., Li, X., Zhang, J. & Zhu, H. (2016) *Rainfall-induced soil slope failure: stability analysis and probabilistic assessment.* Boca Raton: CRC Press. https://doi.org/10.1201/b20116.